

## CONTRASTING P–T PATHS IN ECLOGITES OF THE BETIC OPHIOLITIC ASSOCIATION, MULHACÉN COMPLEX, SOUTHEASTERN SPAIN

ENCARNACIÓN PUGA<sup>§</sup>

*Instituto Andaluz de Ciencias de la Tierra, CSIC–UGRA, Facultad de Ciencias,  
Universidad de Granada, Avda. Fuentenueva s/n, E-18002 Granada, Spain*

JOSÉ MIGUEL NIETO

*Departamento de Geología, Facultad de Ciencias Experimentales,  
Universidad de Huelva, E-21071 Palos de la Frontera, Huelva, Spain*

ANTONIO DÍAZ DE FEDERICO

*Departamento de Mineralogía y Petrología, Facultad de Ciencias, Universidad de Granada,  
Avda. Fuentenueva s/n, E-18002 Granada, Spain*

### ABSTRACT

The Betic Ophiolitic Association of the Mulhacén Complex, in the Betic Cordilleras of southeastern Spain, is composed, as are other Mesozoic Alpine ophiolitic associations derived from the Western Tethys, of disrupted thrust slices of oceanic crust sandwiched into continental units metamorphosed in a subduction-zone environment. In the Mulhacén Complex, Alpine metamorphism can be subdivided, mainly on the basis of textural relationships supported by geological, paleontological and radiometric data, into two main events: a Late Cretaceous – Paleocene eo-Alpine event, which developed under eclogite-facies conditions, and a Late Eocene – Oligocene meso-Alpine event, under albite–epidote amphibolite-facies conditions. The eo-Alpine event was followed by a retrogression stage, leading to glaucophane-schist-facies assemblages, and the meso-Alpine event climax was followed by greenschist-facies conditions. Metabasic rocks from the Cóbдар and Lugros ophiolitic suites show, respectively, the lowest and the highest grades attained during the eo-Alpine metamorphic event in the Betic Ophiolitic Association of the Mulhacén Complex. The conditions of the metamorphic climax correspond to about 14 kbar and 570°C for the Cóbдар metabasic rocks, *i.e.*, at the limit between glaucophane schists and eclogites, and about 21–22 kbar and 675°C for the Lugros suite, which developed under kyanite-bearing eclogite conditions. Eo-Alpine parageneses were partly obliterated during the meso-Alpine event, the climax of which was about 600 ± 25°C and 8.5 ± 0.5 kbar.

*Keywords:* P–T paths, Alpine metamorphism, plurifacial evolution, kyanite-bearing eclogites, Betic Ophiolitic Association, Betic Cordilleras, Spain.

### SOMMAIRE

L'Association Ophiolitique Bétique que montre le complexe de Mulhacén, dans les Cordillères Bétiques du sud-est de l'Espagne, contient, tout comme c'est le cas d'autres suites ophiolitiques alpines mésozoïques dérivées de la marge occidentale de la mer Tethys, des lambeaux de croûte océanique disloqués, insérés dans des unités d'origine continentale métamorphisées dans un milieu de subduction. Dans le complexe de Mulhacén, les effets du métamorphisme alpin peuvent être subdivisés, surtout selon les relations texturales, appuyées par des données géologiques, paléontologiques et radiométriques, en deux événements principaux: le premier, éo-alpin, d'âge crétacé tardif à paléocène, s'est développé aux conditions du faciès écolite, tant que le second, méso-alpin, d'âge éocène tardif à oligocène, témoigne de conditions typiques du faciès amphibolite à albite–épidote. L'événement éo-alpin a été suivi par un stade de rétrogression menant à des assemblages typiques du faciès des schistes bleus à glaucophane, tandis que des conditions typiques du faciès à schistes verts ont suivi l'événement méso-Alpin. Les roches métabasiques des cortèges ophiolitiques de Cóbдар et de Lugros montrent, respectivement, la plus faible et la plus forte intensité de métamorphisme affectant le complexe de Mulhacén de l'Association Ophiolitique Bétique au cours de l'événement éo-alpin. Les conditions atteintes au cours de cet événement étaient d'environ 14 kbar et 570°C dans la suite de roches métabasiques de

<sup>§</sup> E-mail address: epuga@goliat.ugr.es

Cóbdar, et donc à la limite entre les schistes à glaucophane et les écolgites, et environ 21–22 kbar et 675°C dans la suite de Lugros, qui s'est développée aux conditions du faciès écolgite à kyanite. Les assemblages éo-alpins ont été partiellement oblitérés au cours de l'événement méso-alpin, dont la culmination a atteint environ  $600 \pm 25^\circ\text{C}$  et  $8.5 \pm 0.5$  kbar.

(Traduit par la Rédaction)

**Mots-clés:** trajectoires P–T, métamorphisme alpin, évolution à multiples faciès, écolgite à kyanite, Association Ophiolitique Bétique, Cordillères Bétiques, Espagne.

## INTRODUCTION

The Betic Ophiolitic Association (BOA) is the westernmost outcrop of the Mediterranean Ophiolite Belt (Puga 1990). It is exposed discontinuously along about 250 km in the Mulhacén Complex, in southeastern Spain (black dots in Fig. 1). The ophiolite suites of this association consist of metabasic rocks, spatially associated, or not, with meta-ultramafic rocks, and overlain by metasedimentary units, among which some metabasite and serpentinite lenses may be intercalated.

The metabasic rocks are derived from gabbros, often cumulitic, and diabases, with a gradual transition to amygdaloidal metabasalts containing deformed pillow structures (Puga *et al.* 1989a, 1995). Locally, these basic rocks preserve igneous assemblages that show the sequences of crystallization. Geochemical affinities correspond to a tholeiitic suite generated in an E–MORB geological setting; they were only partly obliterated by the Alpine orogenic metamorphism (Bodiniér *et al.* 1987, Puga *et al.* 1989 a, b, 1995, 1999a). This metamorphism developed in the BOA rocks and in the other

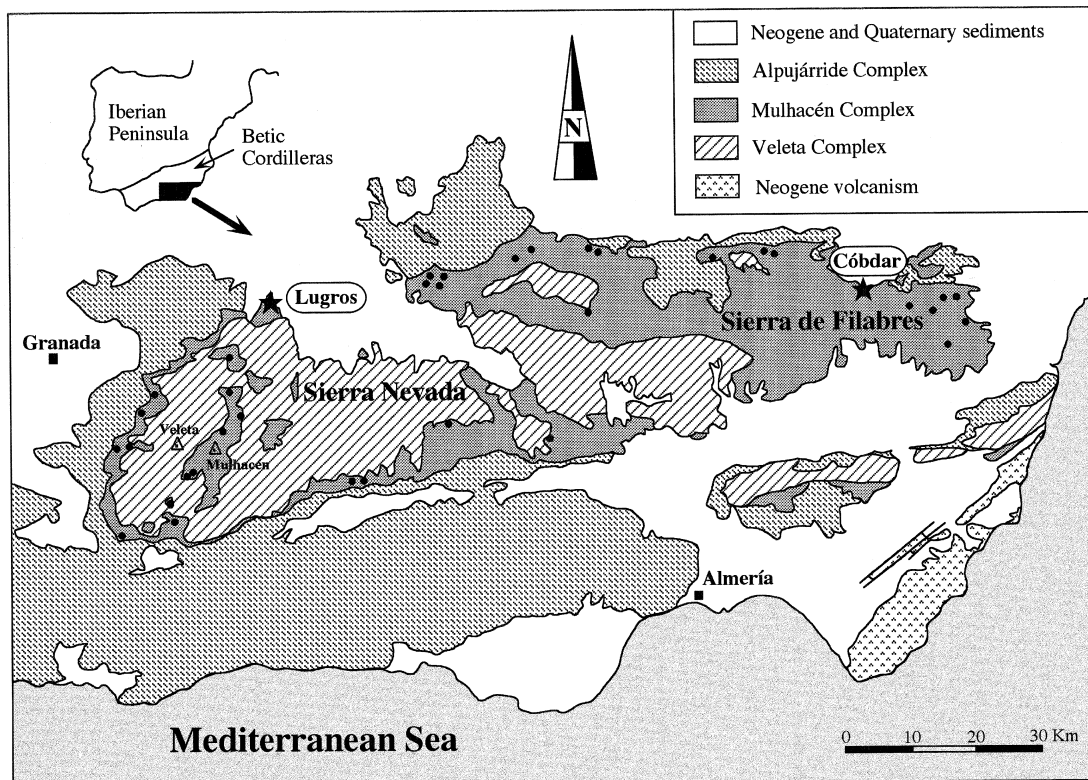


FIG. 1. Geological sketch of the central-eastern sector of the Betic Cordilleras showing the relationships among the Veleta, Mulhacén and Alpujarride complexes, and the location of the Córdar and Lugros ophiolite suites. Solid dots in the Mulhacén Complex represent the location of the main outcrops of the Betic Ophiolitic Association in Sierra Nevada and Sierra de los Filabres. The boundaries between the complexes are drawn according to geological maps (1:50,000 scale) of the MAGNA series and the unpublished data of Díaz de Federico.

units composing the Mulhacén Complex in two main events; the eo-Alpine event involved high-pressure conditions, and the meso-Alpine event involved intermediate-pressure conditions, and each was followed by a stage of retrogression (Puga & Díaz de Federico 1978, Vissers 1981, Bakker *et al.* 1989, Puga *et al.* 1989a, b, 1995, 1999a, De Jong 1991).

The high pressure (HP) attained during the episode of eo-Alpine metamorphism systematically increases from the eastern to the western part of the Mulhacén Complex. The Cóbдар and Lugros metabasite suites (Fig. 1) have been chosen for our comparative study because they have experienced the lowest and the highest metamorphic grade, respectively, attained in the Betic Ophiolite Association. Both suites consist of eclogites and albite–epidote amphibolites derived from volcanic and plutonic rock-types. There exists, nevertheless, a clear contrast in the degree of preservation of the pre-Alpine parageneses (igneous and ocean floor in origin), which is much greater in the Cóbдар suite, and in the physical conditions characterizing the eo-Alpine metamorphism, which attained higher P and T in the Lugros suite. Similar differences also exist between other sequences of ophiolitic metabasic rocks located, respectively, in the eastern and western parts of the Mulhacén Complex (Morten *et al.* 1987, Gómez-Pugnaire & Fernández-Soler 1987, Bakker *et al.* 1989, Puga *et al.* 1989a, b, 1995). These differences have also been identified in exposures of orthogneiss and skarn rocks, located near the villages of Cóbдар and Lugros (Nieto 1996), which form part of the crustal units underlying and overlying the meta-ophiolites (Fig. 2).

Our aim in this paper is to deduce the physical conditions of the successive parageneses present in the Cóbдар and Lugros ophiolitic metabasic rocks, to establish their respective P–T paths, to elucidate the most probable geodynamic environment in which these parageneses developed, as well as to propose a possible interpretation of the different physical conditions attained in the eastern and western parts of the Mulhacén Complex during the eo-Alpine event.

#### GEOLOGICAL SETTING

The BOA forms part of the Mulhacén Complex (Fig. 1), which is exposed in the central and eastern parts of the Internal Zone of the Betic Cordilleras overlying the Veleta Complex (Puga & Díaz de Federico 1978, Díaz de Federico 1980, De Jong 1991). These two metamorphic complexes appear as a series of tectonic windows below the Alpujarride Complex (Fig. 1). The relative location of these complexes and that of the BOA unit in the Mulhacén Complex can be seen in the simplified lithological column of Figure 2, and their description can be found in Torres Roldán (1979), Díaz de Federico *et al.* (1990), Puga *et al.* (1999b, submitted).

The Mulhacén Complex is composed by two thrust units of crustal origin, the Caldera below and the Sabinas above, between which the oceanic BOA unit is tectonically intercalated (Fig. 2). The crustal units are formed of a Paleozoic basement, consisting primarily of graphite-bearing schists containing metagranite lenses and eclogitized skarn rocks, and of a Mesozoic cover, composed of marble, micaceous schists and rhyolitic orthogneisses. The BOA consists of numerous meter-to kilometer-sized lenses of metamorphic rocks, derived from mafic or ultramafic and sedimentary rock-types, similar to those forming some ophiolite suites in the Alps (Desmons 1989). A simplified reconstruction of the various rock-types making up the BOA, with their maximum secondary thickness, is shown in Figure 2. The relative position of the intra-orogenic Soportújar Formation also is represented in this figure. This formation is made up of continental and evaporitic metasedimentary units, and meta-andesitic rocks forming pyroclastic layers and subvolcanic bodies, which were deposited, in a relaxation stage between the eo-Alpine and the meso-Alpine events, upon the other units of the Mulhacén Complex (Fig. 2).

The metabasic rocks of the BOA have been radiometrically dated by Rb/Sr, K/Ar and Ar/Ar. They span the interval from the Triassic–Jurassic boundary to the Upper Jurassic (Hebeda *et al.* 1980, Portugal *et al.* 1988, Puga *et al.* 1991, 1995). In some localities, a high-grade metamorphic assemblage, formed during an ocean-floor stage of metamorphism, has also been partly preserved. A brown amphibole of this assemblage, filling millimetric veins in metabasalts, has been dated by Ar/Ar laser probe as Upper Jurassic (Puga *et al.* 1991, 1995). In the metasedimentary sequence overlying these ophiolites, relics of Cretaceous foraminifera, similar to those found by Lemoine *et al.* (1984) in ophiolites in the Western Alps, have been preserved locally (Tendero *et al.* 1993).

Radiometric age determinations of associations of metamorphic minerals developed during the Alpine orogeny in the Mulhacén Complex are scarce, and their interpretation is in some cases ambiguous, mainly owing to the possible existence of excess Ar in K-bearing minerals, and to Sm/Nd isotopic disequilibrium observed in eclogitic assemblages (Nieto *et al.* 1997a). However, two main events of Alpine metamorphic blastesis can be envisaged from the available data, using K/Ar, Ar/Ar, Rb/Sr and Sm/Nd on whole rocks and mineral separates from the different tectonic units of the Mulhacén Complex (Puga 1976, Portugal *et al.* 1988, Andriessen *et al.* 1991, De Jong 1991, Monié *et al.* 1991, Puga *et al.* 1991, 1995, Nieto *et al.* 1997a): an eo-Alpine Late Cretaceous–Paleocene event, and a meso-Alpine Late Eocene – Oligocene event. The Soportújar Formation was affected only by the meso-Alpine event. Its meta-andesites preserve igneous relics that were dated by K/Ar as Paleocene, and their metamorphic minerals

at Oligocene (Puga *et al.* 1996). During the Miocene, a non-penetrative stage of recrystallization of the previous parageneses and a thermal resetting of most isotopic systems took place, mainly related to ductile extensional tectonic activity (Monié *et al.* 1991).

FIELD OCCURRENCES  
AND PETROGRAPHIC DESCRIPTIONS

The BOA was dismembered and metamorphosed during the Alpine orogeny, as were most of the Mesozoic ophiolitic associations of the Alps (Dietrich 1980, Desmons 1989). Like those associations, the BOA sequences are thus incomplete.

*The Córdar area*

In the Córdar area (Fig. 1), only one sequence of metabasic rocks several km in length and about 200 meters thick, representing the plutonic and volcanic protoliths, and 70 meters of metasediments are preserved (Puga *et al.* 1989a). Scapolite-bearing evaporitic phyllites and carbonate rocks of the Soportújar Formation, affected by the meso-Alpine metamorphism only, overlie the micaceous schists, marbles and calc-schists of the sedimentary sequence of the ophiolites, or its volcanic sequence directly, both affected by the eo-Alpine and meso-Alpine metamorphic events. A few outcrops of metabasalt directly overlain by the Soportújar

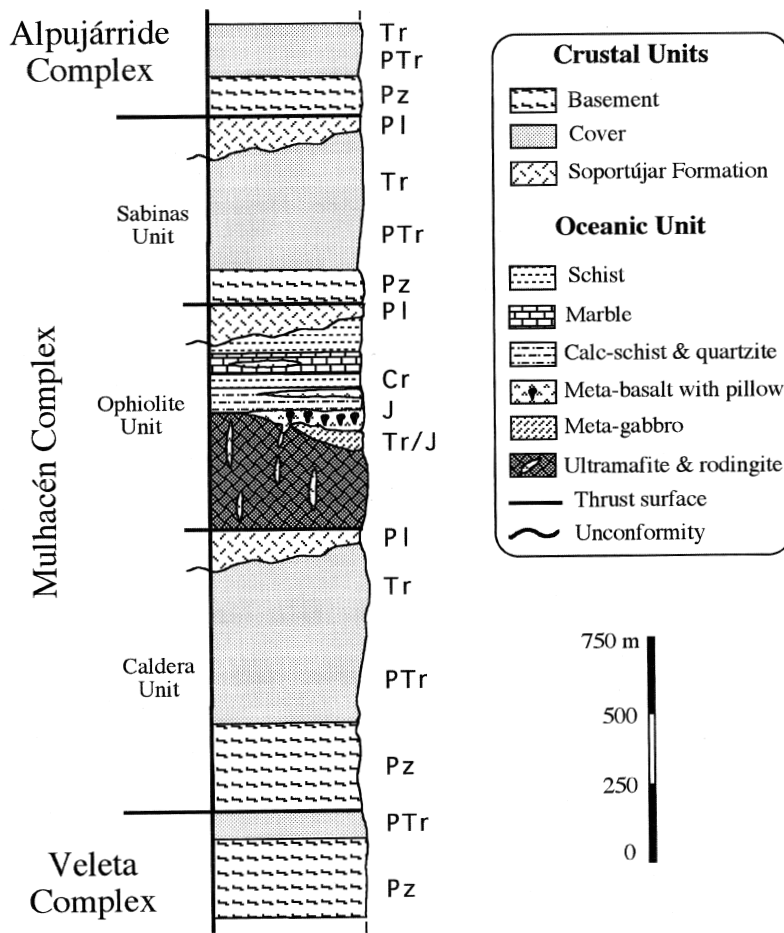


FIG. 2. Simplified lithostratigraphic column of the metamorphic complexes in Figure 1, showing the main rock-types forming the BOA and a reconstruction of their relative position during the primitive oceanic stage. The most probable ages, inferred from radiometric and paleontological data for the different formations making up this column, are indicated as follows: Pz: Paleozoic, PTr: Permo-Triassic, Tr: Triassic, J: Jurassic, C: Cretaceous, Pl: Paleocene.

Formation also have scapolite as late poikiloblasts and filling veins. The ophiolitic association, with or without the overlying Soportujar Formation rocks, is overthrust by marbles and micaceous schists of the Sabinas unit of the Mulhacén Complex (Fig. 2). The volcanic sequence is composed of aphanitic and amygdaloidal metabasalts, some of which preserve flow structures. The basalts, locally cut by several decimeter-thick dykes of diabase, gradually merge into pillow lavas, with sizes ranging from a few decimeters to more than one meter in diameter (Puga *et al.* 1989a). Basaltic layers unconformably overlie different levels of the plutonic sequence, which is formed of alternating horizons of troctolitic cumulates and gabbros, cut across by centimetric to metric dykes of diabase.

The C6bdar metabasalts are generally greenish, very fine-grained and contain numerous millimetric vesicles, which were filled with carbonates in the oceanic environment and have been partially replaced by biotite, chlorite, amphiboles and scapolite in successive metamorphic stages (Puga *et al.* 1989a). The troctolitic cumulates, very common in the C6bdar suite, are dark grey in color, medium grained, and commonly show spheroidal weathering. They alternate with greenish metagabbros having a diabasic texture and a medium to coarse grain-size.

The primary igneous paragenesis, composed of labradorite  $\pm$  forsterite  $\pm$  augite phenocrysts in a plagioclase + clinopyroxene + ore microcrystalline matrix, may be locally preserved in some metabasalts and metagabbros (Fig. 3a). The olivine of this paragenesis commonly is brown, however, owing to exsolution of magnetite during the overimposed ocean-floor and orogenic metamorphic processes (Puga *et al.* 1999a).

The ocean-floor metamorphic process led to some high-T hydrous phases such as brown calcic amphiboles, talc and sheridanite, which fill submicroscopic to millimetric veins and vesicles in basaltic rocks, and partly replace and rim igneous minerals in diabasic and gabbroic lithotypes (Puga *et al.* 1989a). The influx of saline hydrous fluids during this stage has also affected the olivine phenocrysts, in which submicroscopic inclusions bearing NaCl have been identified by electron-microprobe analysis (EMPA) and transmission electron microscopy with analytical electron microscopy (TEM-AEM) (Puga *et al.* 1999a). These hydrous fluids facilitated the exsolution of tiny crystals of amphibole and pyroxene, together with magnetite, in the brownish altered zone of the igneous olivine (Figs. 3a, b), during a stage that began before the development of the orogenic minerals (Puga *et al.* 1999a).

The eo-Alpine metamorphic event developed eclogite or glaucophane schist assemblages only in some metabasic rocks of the C6bdar region. This high-pressure metamorphic process was not very pervasive in the C6bdar ophiolites as is suggested by the local preservation of both the igneous paragenesis and the successive mineral phases that form the eo-Alpine coronitic textures.

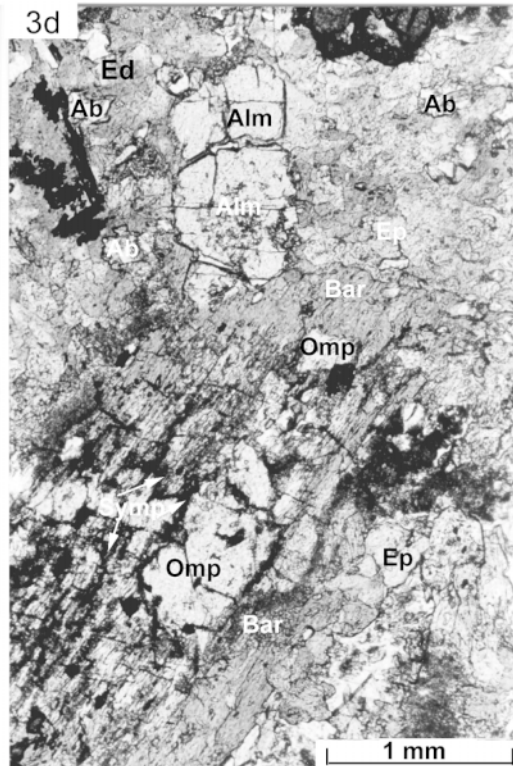
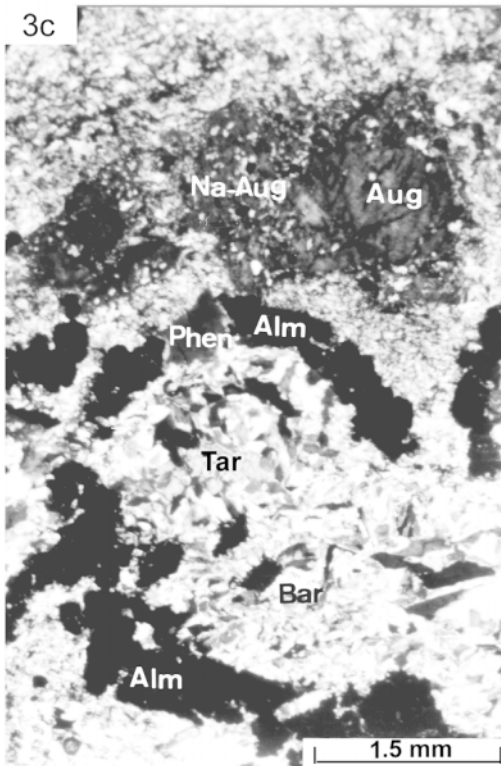
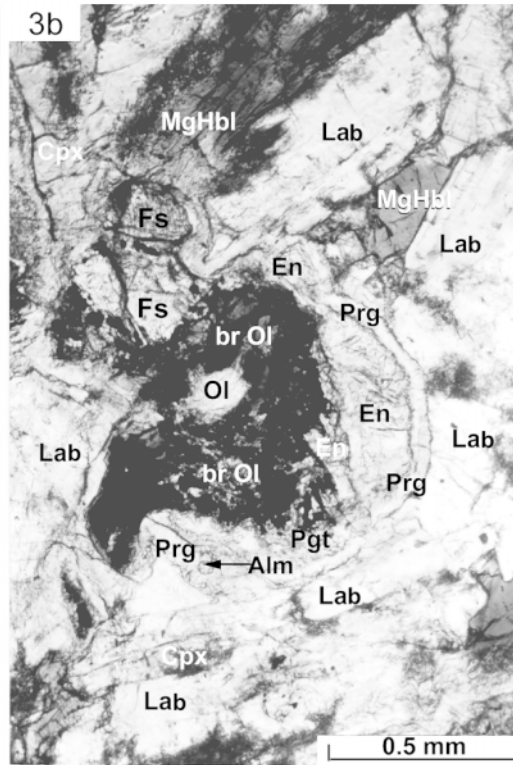
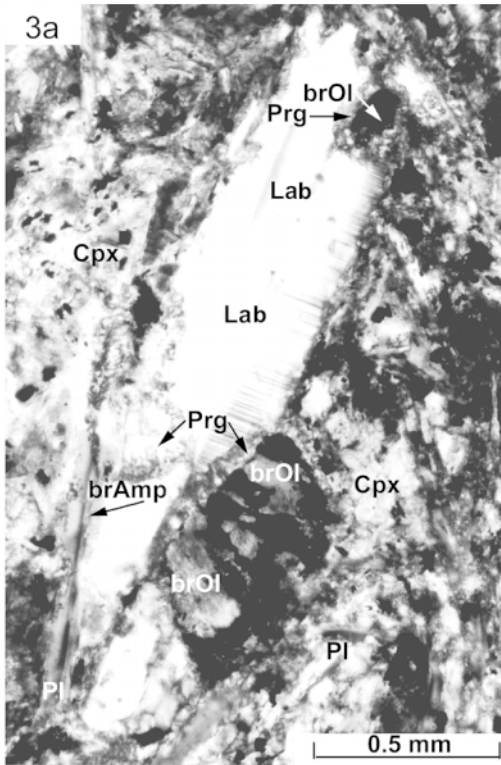
The coronas, shown in Figures 3a to 3c, are developed by reaction of olivine crystals with the surrounding igneous plagioclase, beginning during the prograde stage and attaining the peak conditions of the eo-Alpine event. The following temporal sequence of blastesis in these coronas may be deduced from the textural relationships: (1) crystallization of kelyphitic pargasite at the boundaries of the brownish olivine with the surrounding igneous plagioclase crystals, forming a first external corona (Fig. 3a), (2) replacement of residual olivine by acicular orthopyroxene forming a second discontinuous inner corona (Fig. 3b), (3) replacement of the kelyphitic pargasite by almandine and the acicular orthopyroxene by omphacite, beginning during the prograde eo-Alpine stage and finishing during the peak conditions of this metamorphic event, in the eclogite facies (Fig. 3c), and (4) partial substitution of omphacite and almandine by sodic-calcic amphiboles, and minor opaque minerals and phyllosilicates, during the meso-Alpine event at conditions of the albite-epidote amphibolite facies (Fig. 3c).

In some gabbros and in the dykes of diabase cutting across the volcanic sequence, the eclogitic assemblage omphacite + almandine + rutile  $\pm$  glaucophane  $\pm$  clinozoisite may have been locally formed, developing blastoporphyritic textures (Fig. 3d). Other metamorphic lithotypes, such as glaucophane-bearing omphacitites and clinozoisite-bearing glaucophanites, are also present in the C6bdar meta-ophiolites (Puga *et al.* 1989a).

The eo-Alpine assemblages are only preserved as relics, more or less transformed into the most common meso-Alpine albite-epidote amphibolite assemblage. This assemblage consists of sodic-calcic and calcic amphiboles, which replace omphacite and almandine, with an overgrowth of glaucophane, together with paragonite plus clinozoisite aggregates replacing plagioclase phenocrysts, and epidote and titanite, which overgrow, respectively, clinozoisite and rutile. In this paragenesis, chlorite and micas are also commonly present. The more common textures developed in the meso-Alpine event are the nematoblastic, and the schistose microfolded fabrics, mainly developed in amphibolite layers rich in phyllosilicates. The meso-Alpine albite-epidote amphibolite assemblages may be found, not only replacing the previous eo-Alpine eclogitic parageneses, but even directly formed from the igneous minerals in many metabasic rock samples, which also preserve the igneous fabrics.

#### *The Lugros area*

In the Lugros area (Fig. 1), the ophiolitic association consists of a slice of eclogites, less than 100 meters thick, derived from volcanic and plutonic protoliths, corresponding to three tectonic klippen, several hundred meters to 1 km in length, thrust over garnet-bearing micaceous schists of the Caldera unit and covered by Quaternary deposits (Fig. 2). The plutonic lithotypes,



cross-cut by scarce decimetric dykes of diabase, are predominant in this suite. They consist mainly of olivine-bearing and olivine-free gabbros, locally medium- to coarse-grained, diabasic, and pegmatitic (Cámara 1995). The volcanic sequence is mainly restricted to isolated blocks within an outcrop several hundred meters in extent. Most of these blocks correspond to multiple, irregularly folded layers of basalt, several centimeters in thickness, formed by a quenched outer part, an aphyric black outer zone, and a hypocrySTALLINE central zone. Other blocks in the Lugros suite are formed by piles of molded centimetric minipillows several centimeters in diameter, and decimeter-size pillow lavas. All these structures are the result of submarine eruptions involving recurring small volumes of very fluid magma (Puga *et al.* 1995).

Basic rocks from the Lugros area, as opposed to those from Cóbдар, are entirely transformed into kyanite-bearing eclogites, and less commonly to cofacial garnet glaucophanites; these rocks are only slightly overprinted by albite-epidote amphibolites (Puga *et al.* 1995). In metabasalts present as pillow lavas, the variolitic or porphyritic textures are well preserved, although the igneous phenocrysts and the primary glassy matrix have been completely replaced by metamorphic minerals (Fig. 4a). These volcanic textures, only discernible with parallel light, are largely obliterated by granoblastic recrystallization, only visible with crossed nicols. Scarce relics of brown amphibole, similar to that formed during the ocean-floor stage in the Cóbдар ophiolites, may be found in some samples. It contains abundant tiny exsolved rutile crystals and shows a gradual transition to green sodic-calcic amphibole developed during successive orogenic stages.

The olivine-rich lava flows and gabbros are transformed into coronitic eclogites, in which olivine is replaced by omphacite aggregates surrounded by a rim of almandine, augite is replaced by omphacite + rutile, and calcic plagioclase is replaced firstly by a clinozoisite-paragonite intergrowth and later by omphacite + kyan-

ite aggregates. Veins filled with kyanite  $\pm$  omphacite may be present in these eclogites (Fig. 4b). Omphacite is variably replaced by sodic-calcic amphiboles, mainly barroisite and taramite.

Some Fe- and Na-rich basalts from Lugros (compositions in Puga *et al.* 1995) were transformed into kyanite-bearing eclogites, with glaucophane and paragonite mainly formed during a retrograde eo-Alpine stage. These samples contain also abundant sodic-calcic amphiboles, especially taramite, which developed from the previous minerals, mainly from glaucophane and omphacite, during a younger meso-Alpine overprint (Figs. 4c, d).

Metamorphic structures, mainly meso-Alpine mylonitization bands, are superimposed over the igneous and eo-Alpine ones and locally obliterate them, with the exception of localized low-strain zones. In these less-deformed zones, primary structures are predominant, within decimetric boudins, despite the complete replacement of igneous parageneses by eclogitic ones. The scarcity of amphibolitization in this suite allowed the preservation of some eo-Alpine schistosity, developed by the parallel growth of omphacite and glaucophane prisms, partly included in almandine poikiloblasts.

#### MINERAL CHEMISTRY AND TEXTURAL RELATIONS

Representative results of chemical analyses of the various metamorphic minerals from the Cóbдар and Lugros meta-ophiolites are reported in Tables 1 to 4. The calculated end-members or the corresponding molar proportions are plotted in Figures 5 to 9 (numbers as in the tables), along with other data from the same suites, not shown in these tables for clarity. The paragenetic sequences recognized by microtextural analysis in these meta-ophiolites are shown in Table 5. The minerals and their compositions have been grouped in these tables into different metamorphic events and stages according to textural relationships. The data reported in Tables 1 to 4 were used to establish the P-T paths shown in

FIG. 3. a. Association of primary olivine (br Ol) + plagioclase (Lab) + augitic clinopyroxene (Cpx) preserved as phenocrysts in a Cóbдар metabasalt showing a partly amphibolitized matrix with an intersertal texture. Interstitial brown amphibole in the matrix (br Amp) partially replaces the phenocrysts. Reaction corona of pargasite (Prg) developed between brown olivine (br Ol) and labradorite (Lab). Cantoria to Uleila del Campo road, near Cóbдар village. b. Kelyphitic coronas of pargasite (Prg) (external rim) and acicular pyroxenes (En, Fs, Pgt) (internal zone) partly replacing forsteritic olivine (Ol), colorless in the core and brown toward the border (br Ol), in an amphibolitized metabasalt preserving igneous labradorite (Lab) and clinopyroxene (Cpx). Occasional tiny crystals of almandine-rich garnet (Alm) are formed from pargasite in the external corona. Interstitial brown magnesiohornblende (MgHbl) is partly replaced by green amphibole toward the rims. Rio de los Molinos, Cóbдар region. c. Coronitic texture in an amphibolitized eclogite from olivine-bearing gabbro. Almandine coronas (Alm) replaced kelyphitic pargasite rims (surrounding olivine sites) during the eclogitic stage, and sodic-calcic amphiboles (Bar, Tar) replaced sodic-calcic Cpx aggregates, in paragenetic association with almandine, during the meso-Alpine event. Relics of primary augite partly transformed into sodian augite (Na-Aug), toward the external zone, are still preserved. Path to Cóbдар village from Cantoria to Uleila del Campo road. d. Almandine-omphacite eclogitic paragenesis, partly transformed into an albite-epidote-Na-Ca amphibole assemblage in eclogitized diabase. Omphacite phenoblasts (Omp) were replaced in an initial stage by albite-amphibole symplectite (Symp) (darker in the photo) along fissures and, at a later stage, by barroisite (Bar) and edenite (Ed) phenoblasts, which also were derived from almandine. Same locality as in Figure 3c.

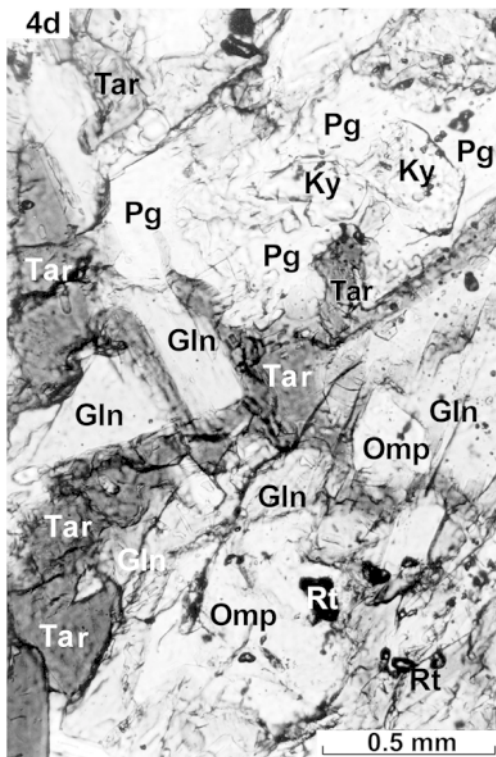
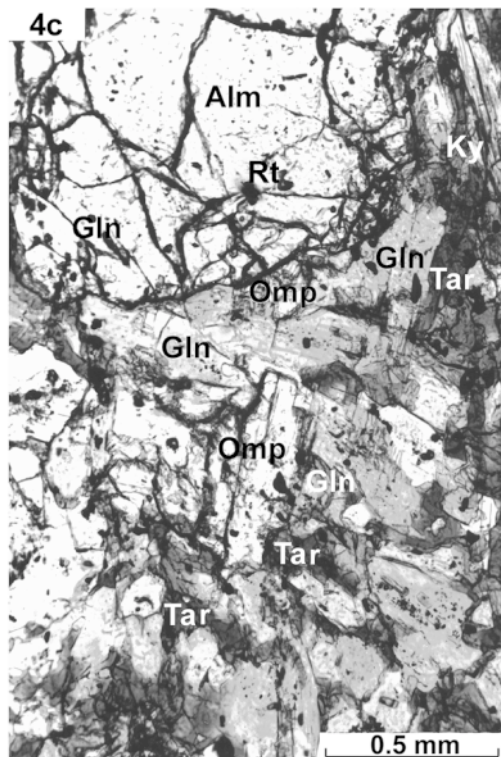
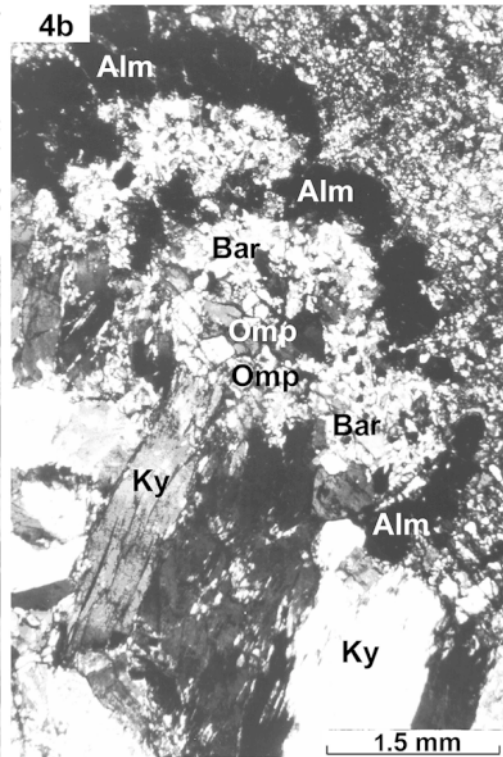
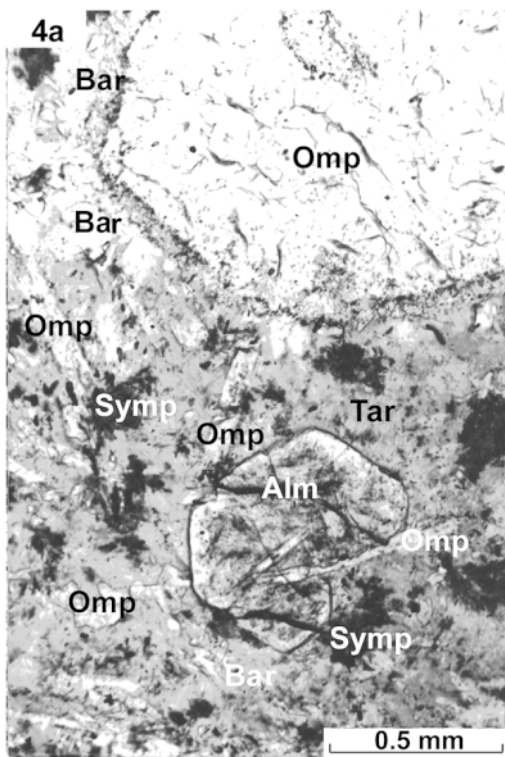


TABLE 1. REPRESENTATIVE RESULTS OF EPMA ANALYSES OF OCEAN-FLOOR AND EO-ALPINE METAMORPHIC MINERALS IN METABASIC ROCKS FROM CÓBDAR

|                                | CB-67              |             | CB-37  |        |       |       | CB-114 |            |        |       |       | CB-36         |               |              |              | CB-51 |       |
|--------------------------------|--------------------|-------------|--------|--------|-------|-------|--------|------------|--------|-------|-------|---------------|---------------|--------------|--------------|-------|-------|
|                                | br Amp<br>in veins | kel.<br>Prg | En     | Pgt    | Omp   | Alm   | Aug    | Na-<br>Aug | Alm    | Czo   | Pg    | Omp 1<br>core | Alm 1<br>core | Omp 2<br>rim | Alm 2<br>rim | Omp 3 | Gln   |
|                                | 1/1                | 1/2         | 1/3    | 1/4    | 1/5   | 1/6   | 1/7    | 1/8        | 1/9    | 1/10  | 1/11  | 1/12          | 1/13          | 1/14         | 1/15         | 1/16  | 1/17  |
| SiO <sub>2</sub> wt%           | 44.03              | 40.53       | 52.97  | 56.50  | 49.50 | 38.95 | 51.39  | 52.08      | 37.48  | 38.75 | 47.36 | 54.17         | 36.41         | 54.51        | 36.79        | 55.06 | 57.65 |
| TiO <sub>2</sub>               | 4.61               | 0.06        | 0.03   | 0.02   | 0.09  | 0.02  | 1.12   | 0.24       | 0.13   | 0.07  | 0.08  | 0.09          | 0.17          | 0.12         | 0.13         | 0.16  | 0.15  |
| Al <sub>2</sub> O <sub>3</sub> | 10.67              | 22.68       | 4.30   | 1.60   | 19.18 | 21.75 | 3.05   | 6.77       | 20.46  | 29.57 | 38.11 | 9.51          | 20.82         | 10.83        | 21.15        | 11.75 | 9.47  |
| Cr <sub>2</sub> O <sub>3</sub> | 0.02               | 0.00        | 0.00   | 0.01   | 0.00  | 0.00  | 0.00   | 0.00       | 0.00   | 0.00  | 0.00  | 0.04          | 0.00          | 0.02         | 0.00         | 0.00  | 0.10  |
| FeO                            | 7.37               | 9.64        | 14.70  | 11.64  | 8.15  | 25.00 | 5.83   | 8.68       | 26.58  | 4.59  | 0.52  | 7.71          | 25.58         | 7.59         | 26.62        | 8.60  | 12.50 |
| MnO                            | 0.06               | 0.12        | 0.45   | 0.20   | 0.11  | 2.56  | 0.14   | 0.10       | 5.26   | 0.14  | 0.00  | 0.07          | 6.60          | 0.08         | 2.80         | 0.11  | 0.05  |
| NiO                            | 0.00               | 0.00        | 0.00   | 0.00   | 0.00  | 0.00  | 0.02   | 0.02       | 0.00   | 0.00  | 0.00  | 0.00          | 0.00          | 0.00         | 0.00         | 0.00  | 0.00  |
| MgO                            | 16.05              | 10.30       | 26.73  | 26.50  | 7.58  | 8.83  | 16.08  | 16.62      | 3.38   | 0.09  | 0.48  | 7.25          | 1.33          | 6.37         | 2.13         | 5.67  | 10.50 |
| CaO                            | 11.95              | 9.30        | 0.13   | 3.04   | 8.64  | 2.87  | 21.80  | 12.41      | 7.00   | 24.17 | 0.18  | 12.67         | 8.47          | 11.44        | 9.91         | 9.07  | 0.98  |
| Na <sub>2</sub> O              | 2.95               | 4.55        | 0.81   | 0.52   | 5.60  | 0.00  | 0.38   | 1.98       | 0.02   | 0.11  | 6.19  | 7.40          | 0.05          | 8.32         | 0.05         | 8.89  | 6.10  |
| K <sub>2</sub> O               | 0.21               | 0.18        | 0.20   | 0.02   | 0.25  | 0.00  | 0.00   | 0.23       | 0.00   | 0.01  | 1.96  | 0.00          | 0.01          | 0.00         | 0.00         | 0.01  | 0.01  |
| Total Oxygen                   | 97.89              | 97.36       | 100.31 | 100.05 | 99.10 | 99.99 | 99.82  | 99.14      | 100.31 | 97.50 | 94.88 | 98.90         | 99.42         | 99.28        | 99.59        | 99.32 | 97.51 |
| Cations                        | 23                 | 23          | 4      | 4      | 4     | 12    | 4      | 4          | 12     | 12.5  | 11    | 4             | 12            | 4            | 12           | 4     | 23    |
| Si <i>apfu</i>                 | 6.34               | 5.85        | 1.88   | 2.02   | 2.00  | 3.00  | 1.89   | 1.90       | 2.97   | 3.03  | 3.05  | 2.00          | 2.94          | 2.00         | 2.93         | 2.00  | 8.01  |
| <sup>IV</sup> Al               | 1.66               | 2.15        | 0.12   | 0.00   | 0.00  | 0.00  | 0.11   | 0.10       | 0.03   | 0.00  | 0.95  | 0.00          | 0.06          | 0.00         | 0.07         | 0.00  | 0.00  |
| <sup>VI</sup> Al               | 0.15               | 1.71        | 0.06   | 0.07   | 0.91  | 1.97  | 0.02   | 0.19       | 1.88   | 2.72  | 1.94  | 0.41          | 1.92          | 0.47         | 1.92         | 0.50  | 1.55  |
| Ti                             | 0.50               | 0.01        | 0.00   | 0.00   | 0.00  | 0.00  | 0.03   | 0.01       | 0.01   | 0.00  | 0.00  | 0.00          | 0.01          | 0.00         | 0.01         | 0.00  | 0.02  |
| Cr                             | 0.00               | 0.00        | 0.00   | 0.00   | 0.00  | 0.00  | 0.00   | 0.00       | 0.00   | 0.00  | 0.00  | 0.00          | 0.00          | 0.00         | 0.00         | 0.00  | 0.01  |
| Fe <sup>3+</sup>               | 0.00               | 0.00        | 0.00   | 0.00   | 0.00  | 0.03  | 0.01   | 0.00       | 0.14   | 0.28  | 0.00  | 0.12          | 0.14          | 0.12         | 0.14         | 0.12  | 0.00  |
| Fe <sup>2+</sup>               | 0.89               | 1.16        | 0.44   | 0.35   | 0.25  | 1.58  | 0.17   | 0.26       | 1.62   | 0.00  | 0.03  | 0.12          | 1.59          | 0.10         | 1.64         | 0.13  | 1.45  |
| Mn                             | 0.08               | 0.02        | 0.01   | 0.01   | 0.00  | 0.17  | 0.00   | 0.00       | 0.35   | 0.01  | 0.00  | 0.00          | 0.45          | 0.00         | 0.19         | 0.00  | 0.01  |
| Ni                             | 0.00               | 0.00        | 0.00   | 0.00   | 0.00  | 0.00  | 0.00   | 0.00       | 0.00   | 0.00  | 0.00  | 0.00          | 0.00          | 0.00         | 0.00         | 0.00  | 0.00  |
| Mg                             | 3.44               | 2.22        | 1.42   | 1.41   | 0.46  | 1.01  | 0.88   | 0.90       | 0.40   | 0.01  | 0.05  | 0.40          | 0.16          | 0.35         | 0.25         | 0.31  | 2.18  |
| Ca                             | 1.84               | 1.44        | 0.01   | 0.12   | 0.37  | 0.24  | 0.86   | 0.48       | 0.59   | 2.02  | 0.01  | 0.50          | 0.73          | 0.45         | 0.85         | 0.35  | 0.15  |
| Na                             | 0.82               | 1.28        | 0.06   | 0.04   | 0.44  | 0.00  | 0.03   | 0.14       | 0.00   | 0.00  | 0.77  | 0.53          | 0.01          | 0.59         | 0.01         | 0.63  | 1.64  |
| K                              | 0.04               | 0.03        | 0.01   | 0.00   | 0.01  | 0.00  | 0.00   | 0.01       | 0.00   | 0.00  | 0.16  | 0.00          | 0.00          | 0.00         | 0.00         | 0.00  | 0.00  |
| f Al                           | 0.08               | 0.44        | 0.35   | 1.00   | 1.00  | 1.00  | 0.15   | 0.65       | 0.98   | 1.00  | 0.67  | 1.00          | 0.97          | 1.00         | 0.97         | 1.00  | 1.00  |

kel.: kelyphitic rim. Na-Aug: sodian augite.

FIG. 4. a. Intermediate zone of a minipillow showing hypidiomorphic almandine poikiloblasts (Alm), including igneous plagioclase microliths, replaced by omphacite (Omp), and clinopyroxene phenocrysts replaced by omphacite plus rutile aggregates, in a matrix preserving the volcanic texture, but formed mainly of omphacite and Na-Ca amphiboles (Bar, Tar). Albite - amphibole - epidote symplectitic intergrowths (Symp) with a rosette-like shape (dark grey in photo) seem to replace quenched crystals of igneous clinopyroxene. Path from Cogollos to Lugros, close to Cerro del Portachuelo. b. Coronitic eclogite resulting from the eo-Alpine metamorphism of an olivine-rich gabbro. Garnet coronas (Alm) surrounding omphacite aggregates (Omp), partly replaced by barroisite (Bar), are cut by a retrograde eo-Alpine kyanite and omphacite vein (Ky), in a matrix mainly consisting of the association epidote + Na-Ca amphibole. c. Kyanite-bearing eclogite rich in glaucophane (Gln), taramite (Tar) and paragonite, which originated from a Fe-rich basalt underlying the minipillows shown in Figure 4a. Almandine poikiloblasts (Alm) (upper part of the photo) contain rutile (Rt), glaucophane and omphacite inclusions, and are also surrounded at equilibrium by the same minerals. Glaucophane is partly transformed to taramite. d. Same thin section as in Figure 4c, showing kyanite (Ky) and omphacite relics (Omp), partly transformed to paragonite (Pg) and glaucophane (Gln), respectively. Taramite (Tar), darker in the photo, surrounds and partly replaces both paragonite and glaucophane.

TABLE 2. REPRESENTATIVE RESULTS OF EPMA ANALYSES OF MESO-ALPINE METAMORPHIC MINERALS IN METABASIC ROCKS FROM CÓBDAR

|                                | CB-37     | CB-9       | CB-1      | CB-114      | CB-36     |           | CB-3       | CB-16        |
|--------------------------------|-----------|------------|-----------|-------------|-----------|-----------|------------|--------------|
|                                | Ed<br>2/1 | Bar<br>2/2 | Ep<br>2/3 | Phen<br>2/4 | Ed<br>2/5 | Ab<br>2/6 | Tar<br>2/7 | gr Bt<br>2/8 |
| SiO <sub>2</sub> wt%           | 45.90     | 48.23      | 38.49     | 47.71       | 42.78     | 67.66     | 41.12      | 39.98        |
| TiO <sub>2</sub>               | 0.08      | 0.24       | 0.00      | 0.31        | 0.50      | 0.00      | 0.33       | 1.33         |
| Al <sub>2</sub> O <sub>3</sub> | 10.07     | 12.87      | 27.74     | 30.71       | 12.96     | 20.60     | 14.24      | 15.91        |
| Cr <sub>2</sub> O <sub>3</sub> | 0.00      | 0.00       | 0.00      | 0.00        | 0.01      | 0.00      | 0.00       | 0.03         |
| FeO                            | 13.79     | 10.03      | 6.47      | 2.12        | 16.84     | 0.00      | 20.81      | 9.89         |
| MnO                            | 0.23      | 0.08       | 0.00      | 0.03        | 0.01      | 0.00      | 0.23       | 0.05         |
| NiO                            | 0.00      | 0.00       | 0.00      | 0.00        | 0.00      | 0.00      | 0.00       | 0.00         |
| MgO                            | 13.70     | 13.21      | 0.00      | 2.61        | 9.24      | 0.00      | 6.68       | 18.11        |
| CaO                            | 10.87     | 8.41       | 23.88     | 0.02        | 9.95      | 1.02      | 7.78       | 0.02         |
| Na <sub>2</sub> O              | 2.95      | 3.57       | 0.00      | 0.87        | 3.44      | 11.20     | 4.10       | 0.28         |
| K <sub>2</sub> O               | 0.07      | 0.45       | 0.00      | 9.75        | 0.80      | 0.05      | 1.23       | 8.92         |
| Total                          | 97.66     | 97.09      | 96.58     | 94.13       | 96.53     | 100.53    | 96.52      | 94.51        |
| Oxygen                         | 23        | 23         | 12.5      | 11          | 23        | 8         | 23         | 12           |
| Si <i>appu</i>                 | 6.51      | 6.84       | 2.94      | 3.22        | 6.44      | 2.95      | 6.24       | 2.83         |
| <sup>IV</sup> Al               | 1.49      | 1.17       | 0.06      | 0.78        | 1.56      | 1.06      | 1.76       | 1.17         |
| <sup>VI</sup> Al               | 0.43      | 0.99       | 2.44      | 1.66        | 0.74      | 0.00      | 0.78       | 0.15         |
| Ti                             | 0.01      | 0.03       | 0.00      | 0.02        | 0.05      | 0.00      | 0.04       | 0.07         |
| Cr                             | 0.00      | 0.00       | 0.00      | 0.00        | 0.00      | 0.00      | 0.00       | 0.00         |
| Fe <sup>3+</sup>               | 1.64      | 0.17       | 0.41      | 0.00        | 0.35      | 0.00      | 0.31       | 0.00         |
| Fe <sup>2+</sup>               | 0.00      | 1.02       | 0.00      | 0.12        | 1.77      | 0.00      | 2.33       | 0.59         |
| Mn                             | 0.03      | 0.01       | 0.00      | 0.00        | 0.01      | 0.00      | 0.03       | 0.00         |
| Ni                             | 0.00      | 0.00       | 0.00      | 0.00        | 0.00      | 0.00      | 0.00       | 0.00         |
| Mg                             | 2.99      | 2.79       | 0.00      | 0.26        | 2.07      | 0.00      | 1.51       | 1.91         |
| Ca                             | 1.65      | 1.28       | 1.95      | 0.00        | 1.61      | 0.05      | 1.26       | 0.00         |
| Na                             | 0.81      | 0.98       | 0.00      | 0.11        | 1.00      | 0.95      | 1.21       | 0.04         |
| K                              | 0.01      | 0.08       | 0.00      | 0.84        | 0.15      | 0.00      | 0.24       | 0.80         |
| fAl                            | 0.22      | 0.46       | 0.98      | 0.68        | 0.32      | 0.00      | 0.31       | 0.11         |

Figure 10. Those corresponding to omphacite–garnet and plagioclase–amphibole pairs, used as geothermometers, are set out in adjacent columns with the same subscripts. The fAl values [= <sup>VI</sup>Al/(<sup>VI</sup>Al + <sup>IV</sup>Al)] proposed by Smith (1988) have been useful in discriminating between the relative pressure conditions of blastesis in the amphiboles and clinopyroxenes of these rocks (see notes at the bottom of tables).

Mineral abbreviations in the tables, figures and throughout the text follow Kretz (1983), with the following additions: Bar barroisite, Krs kaersutite, Lab labradorite, Pgt pigeonite, Phen phengite, Tar taramite and Uv uvarovite. The meaning of some complementary abbreviations in the microphotographs is indicated in the corresponding figure captions. Chemical analyses were performed using a CAMECA SX-50 electron microprobe using natural and synthetic standards. Accelerating voltage was 20 kV and beam current was 15 nA. Coefficients of variation were close to ±1%, ±2.5%, and ±5% for 10 wt.%, 1 wt.%, and 0.25 wt.% analyte concentrations, respectively.

### Garnet

Structural formulae were calculated on a basis of 12 atoms of oxygen and with a Fe<sup>2+</sup>: Fe<sup>3+</sup> ratio inferred on the basis of stoichiometry (Droop 1987). End-members were calculated in the following order: Uv, Adr, Prp, Alm, Sps and Grs. In metabasic rocks from Cóbдар and Lugros, the garnet is almandine-rich ( $0.4 < X_{\text{alm}} < 0.7$ ), but the compositional ranges in the two localities over-

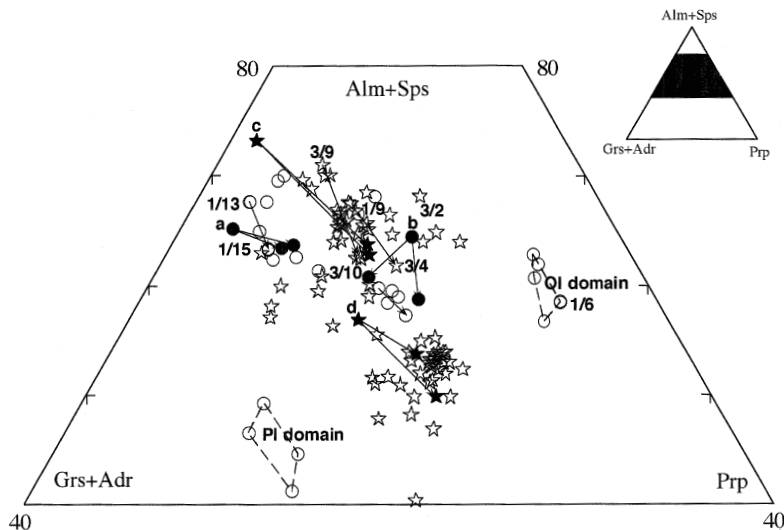


Fig. 5. Composition of garnet in the metabasic rocks from Cóbдар (circles) and Lugros (stars) plotted in terms of the Prp – (Alm + Sps) – (Grs + Adr) components. Arrows join the core and rim of the same crystal. Garnet compositions labeled a, b, c and d, and represented with filled symbols, correspond, respectively, to garnet crystals for which profiles have been represented as a, b, c and d in Figure 6. Numbers correspond to compositions in Tables 1 and 3.

TABLE 3. REPRESENTATIVE RESULTS OF EPMA ANALYSES OF METAMORPHIC EO-ALPINE MINERALS IN ECLOGITES FROM LUGROS

|                                | LG-1       |              | LG-28               |                     |                     | LG-2                |              | LG-3         | LG-20                |                      | LG-28      |             |
|--------------------------------|------------|--------------|---------------------|---------------------|---------------------|---------------------|--------------|--------------|----------------------|----------------------|------------|-------------|
|                                | Czo<br>3/1 | Alm 1<br>3/2 | Omp 1<br>rim<br>3/3 | Alm 2<br>rim<br>3/4 | Omp 2<br>rim<br>3/5 | Omp 3<br>rim<br>3/6 | Omp 4<br>3/7 | Omp 5<br>3/8 | Alm 3<br>core<br>3/9 | Alm 4<br>rim<br>3/10 | Pg<br>3/11 | Gln<br>3/12 |
| SiO <sub>2</sub> wt%           | 38.85      | 37.96        | 56.03               | 37.10               | 54.69               | 56.48               | 55.58        | 52.39        | 37.15                | 37.25                | 46.05      | 57.31       |
| TiO <sub>2</sub>               | 0.05       | 0.06         | 0.07                | 0.11                | 0.08                | 0.08                | 0.19         | 0.12         | 0.13                 | 0.04                 | 0.05       | 0.03        |
| Al <sub>2</sub> O <sub>3</sub> | 28.55      | 21.25        | 11.58               | 21.44               | 11.77               | 11.26               | 12.68        | 11.85        | 20.55                | 20.72                | 39.08      | 10.19       |
| Cr <sub>2</sub> O <sub>3</sub> | 0.03       | 0.02         | 0.00                | 0.03                | 0.00                | 0.02                | 0.01         | 0.03         | 0.00                 | 0.00                 | 0.02       | 0.02        |
| FeO                            | 6.29       | 31.44        | 8.55                | 29.25               | 8.84                | 4.76                | 5.13         | 5.90         | 29.02                | 28.46                | 0.76       | 9.83        |
| MnO                            | 0.03       | 0.50         | 0.01                | 0.41                | 0.02                | 0.03                | 0.03         | 0.00         | 3.80                 | 0.65                 | 0.00       | 0.02        |
| NiO                            | 0.00       | 0.00         | 0.02                | 0.00                | 0.00                | 0.00                | 0.00         | 0.00         | 0.00                 | 0.00                 | 0.00       | 0.03        |
| MgO                            | 0.13       | 4.51         | 5.36                | 4.72                | 5.02                | 8.13                | 6.72         | 9.00         | 2.11                 | 3.85                 | 0.09       | 11.81       |
| CaO                            | 24.18      | 5.01         | 8.46                | 6.67                | 8.21                | 12.46               | 10.80        | 12.47        | 7.15                 | 7.69                 | 0.22       | 1.11        |
| Na <sub>2</sub> O              | 0.01       | 0.03         | 9.13                | 0.03                | 9.31                | 7.27                | 8.34         | 6.35         | 0.00                 | 0.00                 | 7.04       | 6.72        |
| K <sub>2</sub> O               | 0.00       | 0.00         | 0.00                | 0.00                | 0.01                | 0.01                | 0.00         | 0.14         | 0.00                 | 0.00                 | 0.79       | 0.04        |
| Total                          | 98.14      | 100.78       | 99.22               | 99.8                | 97.95               | 100.49              | 99.48        | 98.25        | 99.90                | 98.66                | 94.10      | 97.10       |
| Oxygen Cations                 | 13         | 12           | 4                   | 12                  | 4                   | 4                   | 4            | 4            | 12                   | 12                   | 11         | 23          |
| Si <i>apfu</i>                 | 2.92       | 2.98         | 2.00                | 2.92                | 2.00                | 2.00                | 2.00         | 2.00         | 2.98                 | 2.98                 | 2.99       | 7.93        |
| <sup>IV</sup> Al               | 0.08       | 0.02         | 0.00                | 0.08                | 0.00                | 0.00                | 0.00         | 0.00         | 0.02                 | 0.02                 | 1.01       | 0.07        |
| <sup>VI</sup> Al               | 2.45       | 1.95         | 0.49                | 1.92                | 0.51                | 0.47                | 0.54         | 0.53         | 1.92                 | 1.93                 | 1.97       | 1.59        |
| Ti                             | 0.00       | 0.00         | 0.00                | 0.01                | 0.00                | 0.00                | 0.01         | 0.00         | 0.01                 | 0.00                 | 0.00       | 0.00        |
| Cr                             | 0.00       | 0.00         | 0.00                | 0.00                | 0.00                | 0.00                | 0.00         | 0.00         | 0.00                 | 0.00                 | 0.00       | 0.00        |
| Fe <sup>3+</sup>               | 0.40       | 0.07         | 0.15                | 0.15                | 0.15                | 0.03                | 0.04         | 0.00         | 0.08                 | 0.09                 | 0.00       | 0.00        |
| Fe <sup>2+</sup>               | 0.00       | 1.99         | 0.11                | 1.78                | 0.12                | 0.11                | 0.11         | 0.18         | 1.86                 | 1.82                 | 0.04       | 1.14        |
| Mn                             | 0.00       | 0.03         | 0.00                | 0.03                | 0.00                | 0.00                | 0.00         | 0.00         | 0.26                 | 0.04                 | 0.00       | 0.00        |
| Ni                             | 0.00       | 0.00         | 0.00                | 0.00                | 0.00                | 0.00                | 0.00         | 0.00         | 0.00                 | 0.00                 | 0.00       | 0.00        |
| Mg                             | 0.01       | 0.53         | 0.29                | 0.56                | 0.27                | 0.43                | 0.36         | 0.51         | 0.25                 | 0.46                 | 0.01       | 2.44        |
| Ca                             | 1.95       | 0.42         | 0.32                | 0.56                | 0.32                | 0.47                | 0.42         | 0.51         | 0.61                 | 0.66                 | 0.02       | 0.16        |
| Na                             | 0.00       | 0.01         | 0.63                | 0.00                | 0.66                | 0.50                | 0.58         | 0.47         | 0.00                 | 0.00                 | 0.89       | 1.80        |
| K                              | 0.00       | 0.00         | 0.00                | 0.00                | 0.00                | 0.00                | 0.00         | 0.01         | 0.00                 | 0.00                 | 0.07       | 0.01        |
| fAl                            | 0.97       | 0.99         | 1.00                | 0.96                | 1.00                | 1.00                | 1.00         | 1.00         | 0.99                 | 0.99                 | 0.66       | 0.96        |

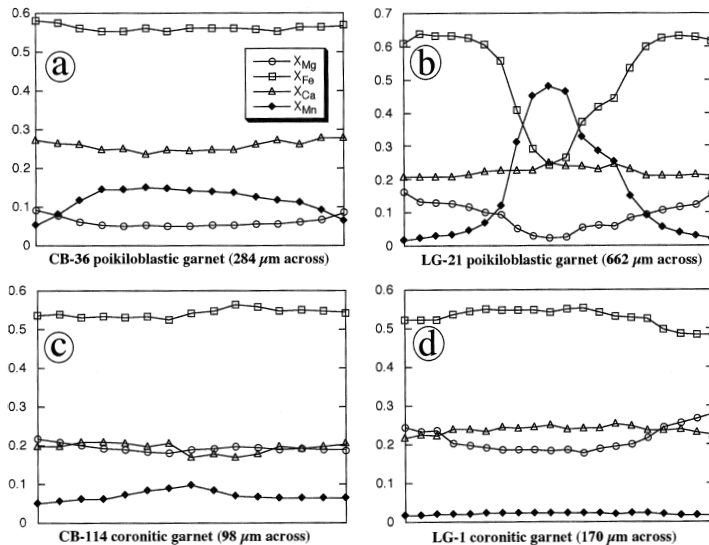


FIG. 6. Representative profiles of garnet crystals in eclogites from Córdar (samples CB-36 and CB-114) and Lugros (samples LG-1 and LG-21).

TABLE 4. REPRESENTATIVE RESULTS OF EPMA ANALYSES OF MESO-ALPINE METAMORPHIC MINERALS IN ECLOGITES FROM LUGROS

|                                | LG-10       |             | LG-28       |               | LG-4        |             |              |
|--------------------------------|-------------|-------------|-------------|---------------|-------------|-------------|--------------|
|                                | Phen<br>4/1 | Tar<br>4/2  | Ab<br>4/3   | Ep<br>4/4     | Ed<br>4/5   | Bar<br>4/6  | gr Bt<br>4/7 |
| SiO <sub>2</sub> wt%           | 49.47       | 40.68       | 68.61       | 37.99         | 45.16       | 49.34       | 38.20        |
| TiO <sub>2</sub>               | 0.46        | 0.28        | 0.02        | 0.08          | 0.43        | 0.33        | 1.31         |
| Al <sub>2</sub> O <sub>3</sub> | 29.78       | 16.01       | 19.58       | 26.72         | 12.48       | 12.34       | 16.05        |
| Cr <sub>2</sub> O <sub>3</sub> | 0.00        | 0.00        | 0.04        | 0.07          | 0.03        | 0.02        | 0.05         |
| FeO                            | 2.47        | 18.76       | 0.06        | 8.13          | 12.76       | 11.39       | 11.67        |
| MnO                            | 0.00        | 0.04        | 0.00        | 0.05          | 0.11        | 0.14        | 0.05         |
| NiO                            | 0.00        | 0.00        | 0.02        | 0.00          | 0.00        | 0.00        | 0.00         |
| MgO                            | 2.73        | 6.31        | 0.00        | 0.09          | 12.51       | 12.43       | 17.73        |
| CaO                            | 0.02        | 7.34        | 0.22        | 23.59         | 10.06       | 7.08        | 0.09         |
| Na <sub>2</sub> O              | 1.13        | 5.12        | 11.58       | 0.02          | 3.21        | 4.24        | 0.19         |
| K <sub>2</sub> O               | 9.46        | 0.98        | 0.03        | 0.01          | 0.37        | 0.24        | 8.24         |
| Total Oxygen                   | 95.52<br>11 | 95.52<br>23 | 100.16<br>8 | 96.76<br>12.5 | 97.12<br>23 | 97.54<br>23 | 93.58<br>12  |
| Si <i>appfu</i>                | 3.29        | 6.22        | 2.99        | 2.92          | 6.55        | 7.05        | 2.70         |
| <sup>IV</sup> Al               | 0.71        | 1.78        | 1.01        | 0.08          | 1.45        | 0.95        | 1.30         |
| <sup>VI</sup> Al               | 1.62        | 1.11        | 0.00        | 2.35          | 0.68        | 1.12        | 0.03         |
| Ti                             | 0.02        | 0.03        | 0.00        | 0.00          | 0.05        | 0.04        | 0.07         |
| Cr                             | 0.00        | 0.00        | 0.00        | 0.00          | 0.00        | 0.00        | 0.00         |
| Fe <sup>3+</sup>               | 0.00        | 0.52        | 0.00        | 0.52          | 0.19        | 0.00        | 0.00         |
| Fe <sup>2+</sup>               | 0.14        | 1.88        | 0.00        | 0.00          | 1.36        | 1.36        | 0.69         |
| Mn                             | 0.00        | 0.01        | 0.00        | 0.00          | 0.01        | 0.02        | 0.00         |
| Ni                             | 0.00        | 0.00        | 0.00        | 0.00          | 0.00        | 0.00        | 0.00         |
| Mg                             | 0.27        | 1.44        | 0.00        | 0.01          | 2.71        | 2.65        | 1.87         |
| Ca                             | 0.00        | 1.20        | 0.01        | 1.95          | 1.56        | 1.08        | 0.01         |
| Na                             | 0.15        | 1.52        | 0.98        | 0.00          | 0.90        | 1.17        | 0.03         |
| K                              | 0.80        | 0.19        | 0.00        | 0.00          | 0.07        | 0.04        | 0.74         |
| fAl                            | 0.69        | 0.38        | 0.00        | 0.97          | 0.32        | 0.54        | 0.02         |

lap only partially (Fig. 5). Most samples plot in the range  $X_{\text{Grs}} + X_{\text{Adr}}$  between 0.20 and 0.30.

In the meta-ophiolite suite of C6bdar, grains of garnet present in the rare eclogites tend to be poikiloblasts, less than one millimeter in size, with inclusions mainly of rutile and epidote. They are slightly zoned, as shown in Table 1 and Figure 5, with compositions 1/13 (core) and 1/15 (rim) of a garnet from the eclogite sample CB-36. The pyrope and grossular contents of this garnet and, to a lesser extent, the almandine content, increase from core to rim, whereas the spessartine content decreases to half its value (Fig. 6a). This type of zoning is interpreted as due to fractionation during growth (Tracy *et al.* 1976). The garnet in this sample forms hypidiomorphic crystals that coexist in equilibrium with omphacite, although both minerals have been partly transformed during the meso-Alpine event, giving place to the albite-epidote amphibolite assemblage (Fig. 3d). The rim of these garnet crystals is homogeneous in composition, as it is shown in Figures 5 and 6a.

The garnet grains forming coronas that surround olivine crystals, now replaced by clinopyroxene and amphibole, have a higher pyrope content than the poikiloblasts previously described (Fig. 6b). The composition of the rims is less homogeneous in the corona

garnet than in the poikiloblasts (Figs. 5, 6b), being richer in pyrope or grossular depending on proximity to olivine or plagioclase, respectively.

The other two compositional fields of garnet represented in Figure 5 correspond to crystals that are richer in pyrope or grossular, respectively. These garnet grains form tiny crystals derived from the kelyphitic coronas of pargasite developed by reaction of igneous olivine and plagioclase in metabasic rocks that preserve relics of their igneous paragenesis (Fig. 3b). The grains of garnet richer in pyrope (composition 1/6) developed in olivine microdomains from kelyphitic coronas of pargasite, whereas garnet richer in grossular developed in the plagioclase microdomains surrounding these coronas. This type of garnet represents local equilibrium reached during the prograde eo-Alpine stage.

Grains of garnet from the Lugros eclogites tend to be hypidiomorphic crystals, less than one millimeter in size in the meta-pillow lavas (Fig. 4a) and coronitic eclogites (Fig. 4b), but reaching locally up to several millimeters in some eclogite horizons deriving from various igneous lithotypes (Fig. 4c).

The garnet formed in eclogites deriving from lithotypes without olivine phenocrysts is granoblastic or porphyroblastic and never forms coronitic textures. This type of garnet is normally poikiloblastic and presents numerous inclusions of rutile, epidote, glaucophane, quartz and, toward the periphery of grains, omphacite. The composition of the garnet depends upon bulk-rock composition more than upon microdomain composition; the almandine content increases with the FeO content of the rock (Puga *et al.* 1995). The zoning is generally similar to the one described in the C6bdar samples, with an increase in pyrope and almandine content and a decrease in the spessartine content from core to rim, although it is more marked in the Lugros suite (compositions 3/9, 3/10, Fig. 5). In some grains of garnet, a stronger zoning has been preserved. The core presents, in these cases, a composition much richer in spessartine and also in grossular, compensated with minimal values in almandine and pyrope, with respect to the composition of the rims (Figs. 5, 6c). This pattern of zoning suggests an increase of P and T conditions during the growth of garnet (Tracy *et al.* 1976), which is compatible with their development during the prograde eclogitic stage. The composition of the rim of garnet poikiloblasts in the Lugros eclogites is, in general, richer in pyrope and almandine, and lower in grossular and spessartine, than in the similar type of garnet from the C6bdar eclogites (Figs. 6a, c).

The coronitic garnet in Lugros eclogites (Fig. 4b) presents in general a similar compositional range and type of zoning to those of the poikiloblasts in these rocks (Figs. 5, 6d), suggesting that equilibrium has been attained during the development of these coronas. The pyrope content of the coronitic garnet is, however, distinctly greater, and the almandine content slightly lower, than in the poikiloblasts. These chemical differences are

also shown between the coronitic and the poikiloblastic garnet from the C6bdar eclogites, providing evidence of the influence of the pre-existing forsterite crystals in the composition of the garnet coronas developed surrounding these igneous microdomains (Figs. 6b, d).

### Pyroxenes

The structural formulae of the pyroxenes were calculated on the basis of four cations, with a  $\text{Fe}^{2+}:\text{Fe}^{3+}$  ratio inferred according to Cawthorn & Collerson (1974) for quadrilateral pyroxenes, and according to Carpenter (1979) for sodic pyroxenes. The proportions of jadeite, aegirine and quadrilateral end-members were calculated according to Morimoto (1988).

Representative composition of pyroxene from C6bdar are set out in Table 1. The composition range is greater than for the Lugros pyroxenes (Fig. 7) owing to: a) the local preservation of relics of igneous clinopyroxene, and b) the development of metamorphic pyroxenes formed at various stages of metamorphism (Table 5).

Igneous-textured clinopyroxenes (Fig. 3c) locally retain an augite core (anal. 1/7) rimmed by metamorphic *sodian augite* (anal. 1/8), which shows notably lower Ti and higher fAl values (Table 1) and jadeite contents (Fig. 7).

Igneous olivine may be partly replaced by acicular *orthopyroxene* forming an inner irregular corona surrounded by kelyphitic pargasite (Fig. 3b). The compo-

sition of this orthopyroxene varies from enstatite, with  $X_{\text{Mg}} = 0.75$  (anal. 1/3), to ferrosilite, with  $X_{\text{Mg}} = 0.4$ . The wollastonite content is locally slightly greater than 5%, corresponding to pigeonite (anal. 1/4, with  $X_{\text{Ca}} = 0.006$ ). In samples showing a more advanced stage of eclogite-facies metamorphism, in which olivine relics are not preserved, orthopyroxene is replaced by omphacite, and the pargasite forming the external coronas is replaced by almandine.

*Omphacite* replacing igneous augite has an Ae content ranging from 10 to 20 mol.%, whereas the Jd content varies from 25 to 50 mol.% in the eclogites (anal. 1/12 and 1/14, Fig. 7) and is near 50 mol.% (Anal. 1/16) in the omphacitites with glaucophane, which originated from plagioclase-rich basalts (Puga *et al.* 1989a). Zoning is difficult to evaluate owing to the small size of the grains, but the proportion of the jadeite component tends to increase toward the rim (Fig. 7).

*Omphacite* is the only clinopyroxene represented in the Lugros samples, with a jadeite content from 30 to 64 mol.% (Fig. 7) and aegirine from 0 to 20 mol.%. *Omphacite* composition is related to bulk-rock composition (Puga *et al.* 1995), with the highest aegirine content in omphacite from a Fe- and Na-rich basalt (LG-28), which also contains the most almandine-rich garnet. *Omphacite* compositions do not vary with the igneous minerals that this clinopyroxene replaces, as shown in Table 3, in which compositions 3/6, 3/7 and 3/8, all rather similar, correspond to omphacite replacing, respectively, olivine, plagioclase phenocryst and plagioclase microlith in the groundmass. Zoning in omphacite from Lugros is more irregular than in that from C6bdar, but also is rather subtle, as is indicated by the arrows in Figure 7.

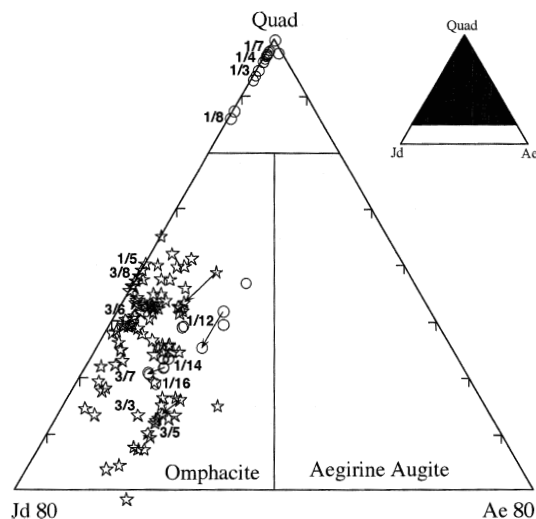


FIG. 7. Clinopyroxene composition in the metabasic rocks from C6bdar (circles) and Lugros (stars) plotted on the Quad-Jd-Ae triangular diagram of Morimoto (1988). Key to arrows and numbers as in Figure 5.

### Amphiboles

Structural formulae were calculated on the basis of 23 atoms of oxygen according to the chemical and crystallographic constraints of Robinson *et al.* (1982). Amphibole is the most abundant metamorphic mineral in the C6bdar metabasic rocks, whereas pyroxene and garnet prevail in the ones from Lugros. Amphiboles are rather similar in the two suites (Figs. 8, 9), although the calcic types are more abundant in C6bdar, and the sodic and sodic-calcic types predominate in Lugros.

In the metavolcanic rocks of the C6bdar suite, the *ocean-floor amphibole* is mainly a brown kaersutite, present in millimetric veins, filling vesicles, or replacing interstitial clinopyroxene in the matrix. This type of amphibole is represented by composition 1/1 (Table 1), which contains 0.5 Ti and 6.34 Si *apfu*. It has a higher  $\text{IV Al}$  content as well as lower  $\text{Na}^{\text{M4}}$  (Fig. 8) and fAl values (anal. 1/1) compared to the other amphibole types present in these rocks, which is consistent with its higher-T and lower-P conditions of genesis. Other brown amphiboles formed in this oceanic stage, such as pargasite and magnesiohornblende, are zoned to more silicic green or blue-green sodic-calcic amphiboles at

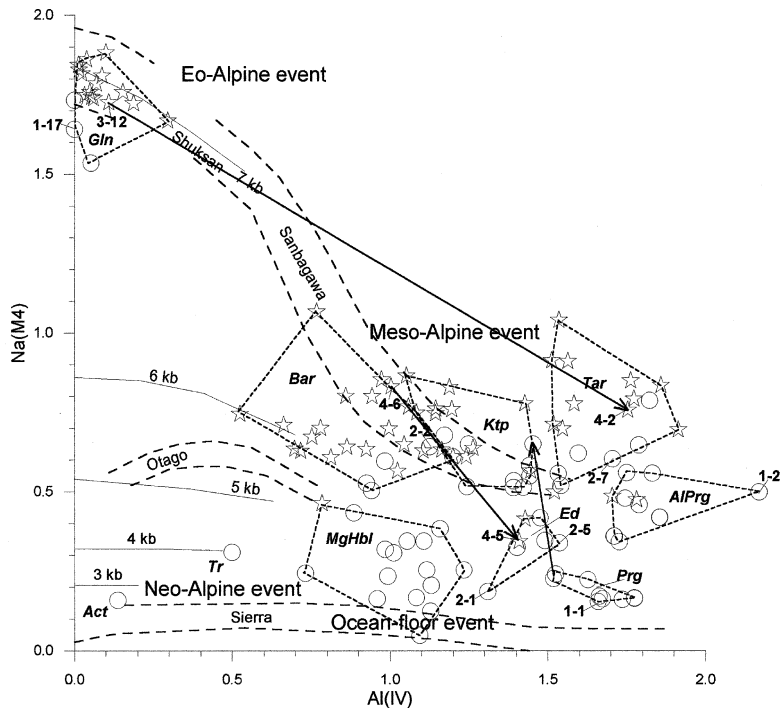


Fig. 8. Plot of the different types of amphibole in the metabasic rocks from C6bdar (circles) and Lugros (stars) plotted on the diagram of Brown (1977), with a tentative estimate of pressure and temperature according to  $\text{Na}^{M4}$  versus  $^{\text{IV}}\text{Al}$  apfu. Arrows represent zoning or overgrowth of some amphiboles. Numbers correspond to compositions in Tables 1 to 4.

the rims (upward-pointing arrow in Figs. 8, 9) during the orogenic conditions.

In the olivine gabbro and diabase, affected only by incipient Alpine metamorphism, kelyphitic *aluminian pargasite* was generated as a reaction rim between olivine and plagioclase. This amphibole coexists with acicular orthopyroxene and precedes almandine and omphacite (Figs. 3a, b). It has a lower  $\text{SiO}_2$  content and a higher  $\text{Al}_2\text{O}_3$  content (anal. 1/2) than texturally later aluminian pargasite and ferroan pargasite (Fig. 8). The other amphibole type developed during the eo-Alpine event is *glaucophane* (anal. 1/17). It is present in two textural situations: as inclusions in garnet, together with omphacite inclusions and, more commonly, replacing this pyroxene in the post-eclogitic stage. Glaucophane is overgrown by barroisite or taramite of the amphibole paragenesis.

Most of the amphiboles in these rocks were formed during the albite-epidote amphibolite stage (Table 5), either by transformation of the eclogitic paragenesis or of the igneous relics that were not metamorphosed during the previous stages of metamorphism. Igneous plagioclase and clinopyroxene (Figs. 3a, b) may be partially

transformed into brown or green *magnesiohornblende*. The orogenic amphiboles present lower Ti and  $^{\text{IV}}\text{Al}$  contents and higher fAl and  $\text{Na}^{M4}$  values than the ocean-floor amphiboles, and commonly rim them. The more common amphibole types developed during the meso-Alpine event are: edenite or aluminian pargasite (among calcic types) and barroisite, katophorite or taramite (among the sodic-calcic types). The calcic amphiboles are more abundant in C6bdar ophiolites than the sodic-calcic ones (Figs. 8, 9).

In eclogites, *barroisite* replaces omphacite derived from olivine or igneous-textured clinopyroxene; in the latter case, it contains abundant inclusions of rutile (Fig. 3d). Locally barroisite is found rimming *katophorite*. Values of fAl in barroisite are higher than in the other sodic-calcic amphiboles (anal. 2/2), suggesting its formation below the highest-pressure conditions. *Edenite* (anal. 2/5) rims barroisite in some crystals, but commonly both types of amphiboles are in contact with coeval albite poikiloblasts, enabling the use of these pairs for the amphibole-plagioclase geothermometer. Blue *taramite* is present in the form of poikiloblasts, larger than 1 mm, in amphibolitized metabasalts. The  $\text{Na}^{M4}$

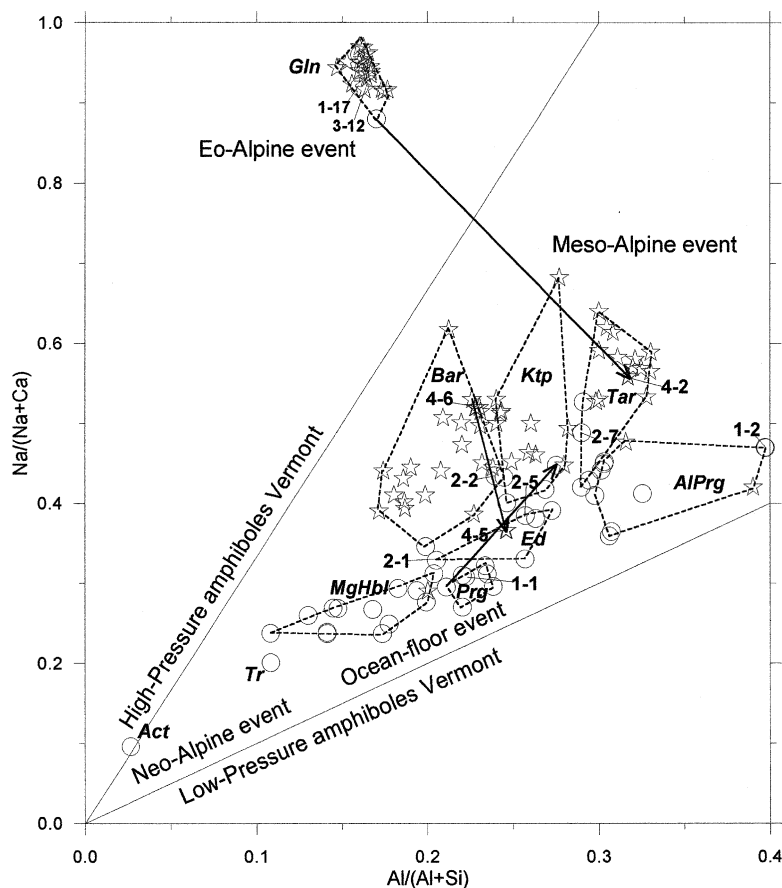


FIG. 9. Compositions of the different types of amphiboles from Cóbдар (circles) and Lugros (stars) plotted on the diagram of Laird & Albee (1981), showing different metamorphic gradients as a function of  $\text{Na}/(\text{Na} + \text{Ca})$  versus  $\text{Al}/(\text{Al} + \text{Si})$  (molar values). Key to arrows and numbers as in Figure 7.

values are similar to those of barroisite (anal. 2/7), and  $^{\text{IV}}\text{Al}$  values are higher than in katophorite and barroisite but similar to those of the aluminian pargasite (Fig. 8).

Texturally younger amphiboles are tremolite and actinolite, which show lower  $\text{Na}^{\text{M4}}$  and  $^{\text{IV}}\text{Al}$  than the other orogenic types (Fig. 8) and are associated with green biotite, phengite, epidote and chlorite (Table 5).

Sodic and sodic-calcic amphiboles are the most abundant types in the Lugros metabasic rocks (Figs. 8, 9). Some relics of brown ocean-floor calcic amphibole can be found lining the vesicles of metapillows. Glaucophane occurs as inclusions in some garnet poikiloblasts, but most commonly replaces omphacite (Figs. 4c, d). This amphibole has similar textural characteristics and composition to the Cóbдар glaucophane (Figs. 8, 9). In the amphibolitized eclogites, glaucophane is probably transformed at the rim to taramite (Figs. 4c, d); Composition 3/12 corresponds to a glaucophane

core, and composition 4/2, to its transformation-induced rim of taramite during the meso-Alpine event (Figs. 8, 9). Barroisite is very well represented in Lugros, mainly replacing omphacite in the former olivine domains of some basalts and gabbros transformed into amphibolitized eclogites (Figs. 4a, b). This amphibole (anal. 4/6) has been found rimmed by edenite (anal. 4/5) with lower  $\text{Na}^{\text{M4}}$  and fAl. Downward-pointing arrows in Figures 8 and 9 represent this zoning, which would indicate development of edenite during a retrograde stage, with a decrease in P, from the meso-Alpine climax in which barroisite was stable. This amphibole is also found rimming katophorite with lower  $\text{Na}^{\text{M4}}$  and fAl values, indicating a change in composition during the prograde meso-Alpine stage. Magnesian hornblende and aluminian pargasite, also replacing omphacite, are less abundant in the Lugros than in the Cóbдар metabasic rocks (Figs. 8, 9).

TABLE 5. RELATIVE SUCCESSION OF STAGES OF BLASTESIS IN ECLOGITES OF THE CÔBDAR AND LUGROS SUITES

| Metamorphic events      | Ocean-floor | Eo-Alpine |          |                    | Meso-Alpine       | Neo-Alpine  |
|-------------------------|-------------|-----------|----------|--------------------|-------------------|-------------|
| Stages                  | Amphibolite | Prograde  | Eclogite | Glaucophane schist | Ab-Ep Amphibolite | Greenschist |
| <b>COBDAR ECLOGITES</b> |             |           |          |                    |                   |             |
| Brown Amphibole         | Abundant    |           |          |                    |                   |             |
| Talc, Phi, Chl          | Scarce      |           |          |                    |                   |             |
| Lawsonite               |             | Probable  |          |                    |                   |             |
| Paragonite              |             | Abundant  |          | Abundant           | Abundant          |             |
| Epidote                 |             | Abundant  |          | Abundant           | Abundant          |             |
| Glaucophane             |             | Abundant  |          | Abundant           |                   |             |
| Quartz                  |             | Abundant  | Abundant |                    |                   |             |
| Kelyphitic Prg          | Abundant    |           |          |                    |                   |             |
| Kelyphitic Opx          | Abundant    |           |          |                    |                   |             |
| Sodian Augite           | Abundant    |           |          |                    |                   |             |
| Omphacite               |             |           | Abundant |                    |                   |             |
| Almandine               |             |           | Abundant |                    |                   |             |
| Rutile                  |             |           | Abundant |                    |                   |             |
| Phengite                |             |           |          | Abundant           | Abundant          | Abundant    |
| Pargasite               |             |           |          |                    | Abundant          |             |
| Edenite                 |             |           |          |                    | Abundant          |             |
| Magnesiohornblende      |             |           |          |                    | Abundant          |             |
| Barroisite              |             |           |          |                    | Abundant          |             |
| Taramite                |             |           |          |                    | Abundant          |             |
| Albite                  |             |           |          |                    | Abundant          | Abundant    |
| Titanite                |             |           |          |                    | Abundant          | Abundant    |
| Scapolite               |             |           |          |                    | Abundant          | Abundant    |
| Actinolite, Tremolite   |             |           |          |                    | Abundant          | Abundant    |
| Green-Biotite           |             |           |          |                    | Abundant          | Abundant    |
| Chlorite                |             |           |          |                    | Abundant          | Abundant    |
| <b>LUGROS ECLOGITES</b> |             |           |          |                    |                   |             |
| Brown Amphibole         | Abundant    |           |          |                    |                   |             |
| Lawsonite               |             | Probable  |          |                    |                   |             |
| Paragonite              |             | Abundant  |          | Abundant           | Abundant          |             |
| Epidote                 |             | Abundant  |          | Abundant           | Abundant          |             |
| Glaucophane             |             | Abundant  |          | Abundant           |                   |             |
| Quartz                  |             | Abundant  | Abundant |                    |                   |             |
| Omphacite               |             |           | Abundant |                    |                   |             |
| Almandine               |             |           | Abundant |                    |                   |             |
| Rutile                  |             |           | Abundant |                    |                   |             |
| Kyanite                 |             |           | Abundant | Abundant           |                   |             |
| Phengite                |             |           |          | Abundant           | Abundant          | Abundant    |
| Aluminopargasite        |             |           |          |                    | Abundant          |             |
| Edenite                 |             |           |          |                    | Abundant          |             |
| Magnesiohornblende      |             |           |          |                    | Abundant          |             |
| Barroisite              |             |           |          |                    | Abundant          |             |
| Katophorite             |             |           |          |                    | Abundant          |             |
| Taramite                |             |           |          |                    | Abundant          |             |
| Albite                  |             |           |          |                    | Abundant          | Abundant    |
| Titanite                |             |           |          |                    | Abundant          | Abundant    |
| Actinolite, Tremolite   |             |           |          |                    | Abundant          | Abundant    |
| Green Biotite           |             |           |          |                    | Abundant          | Abundant    |
| Chlorite                |             |           |          |                    | Abundant          | Abundant    |

Abundant
  Scarce
  Probable

*Epidote*

Structural formulae of epidote-group minerals were calculated on the basis of 12.5 atoms of oxygen and all the iron as Fe<sup>3+</sup>. Piemontite, epidote and clinozoisite

end-members were calculated in that order. This mineral group is represented in all the Alpine stages of blastesis (Table 5).

Different types of epidote with Ep contents between 25 and 56 mol.% are present in the metabasic rocks from

Cóbdar. Those with lower Fe (epidote component between 25 and 30 mol.%) occur in epidote–paragonite intergrowths (anal. 1/10 and 1/11) that replaced igneous calcic plagioclase phenocrysts, whereas those with higher Fe are found in a texturally younger assemblage with amphibole and albite. In the pillow lavas, prismatic epidote replaced the plagioclase microliths forming variolites. Albite–clinozoisite assemblages are common in the vesicles, together with sodic-calcic or calcic amphibole, scapolite and green biotite.

In the metabasic rocks from Lugros, epidote compositions are also richer in clinozoisite in the texturally older Alpine parageneses. A composition very rich in epidote (up to 85 mol.%) has, however, been found as inclusions in garnet of eclogites derived from a basaltic protolith very rich in Fe<sup>2+</sup> (Fig. 4c). Microphenocrysts of plagioclase in basalt, diabase and gabbro were transformed initially into fibrous aggregates of clinozoisite ± paragonite, and then replaced by omphacite, almandine and kyanite during the eclogite-facies climax. Clinozoisite is also abundant as porphyroblasts, with about 40 mol.% epidote (anal. 3/1) at the surface of the pillow lavas and lava flows, probably owing to a greater abundance of fluid in these zones. Texturally later epidote, with 50 to 60 mol.% epidote, is commonly included in albite and amphibole poikiloblasts, and may also form a thin rim around paragonite crystals (anal. 4/4).

#### Micas

Micas are not abundant in the metabasic rocks from the Cóbdar and Lugros suites, except in some Na-rich basalts and intrapillow material probably derived from hyaloclastites. In these rock types, a white mica is associated with chlorite. In both suites, paragonite predominates over phengite, and green biotite contain 60–70 mol.% phlogopite.

Composition 1/11 corresponds to *paragonite* intergrown with clinozoisite; the assemblage replaces igneous plagioclase in an olivine gabbro from Cóbdar. Such a mica has a very narrow compositional range, about 80–85 mol.% paragonite, and high fAl values (0.66 to 0.69) (Table 1). Composition 2/4 corresponds to a *phengite* forming part of a garnet corona (Fig. 3c) from the same gabbro horizon as the paragonite. This mica, with Si between 3.22 and 3.25 *apfu* and high fAl values (Table 2), results from the partial replacement of almandine in the albite–epidote amphibolite stage, during which the omphacite in the inner zone of the corona was also replaced by taramite and barroisite (Fig. 3c).

*Biotite* is more abundant in the Cóbdar metabasic rocks than in those from Lugros (Table 5). It commonly fills vesicles of metabasalts and pillow lavas, together with scapolite, chlorite and amphibole, which replace the pre-existing carbonate in these vesicles. Composition 2/8 contains 64 mol.% phlogopite and 20 mol.% annite, and has a very low fAl value (Table 2).

*Paragonite* is the most abundant mica in the Lugros metabasic rocks. It mainly formed during the prograde and retrograde stages of the eo-Alpine event (Table 5). In the pillow lavas, paragonite together with clinozoisite, which formed during the prograde eclogitic stage, are concentrated toward the pillow rims, and present chemical compositions similar to paragonite formed in the eo-Alpine prograde stage in Cóbdar. In the metabasalts, the eo-Alpine paragonite forms millimetric porphyroblasts partly transformed into barroisite and edenite, or surrounded by a clinozoisite rim. Paragonite is also formed as a replacement product of kyanite during the retrograde eo-Alpine stage (anal. 3/11), and it is commonly transformed into meso-Alpine taramite at the rim (Fig. 4d). *Phengite*, with Si between 3.28 and 3.33 *apfu* in these metabasic rocks, replaces garnet from the coronas in the olivine microdomains, or appears as small crystals (anal. 4/1) following the preferred orientation of sodic-calcic amphiboles. Green *biotite* has been identified in eclogites highly retrograded to albite–epidote amphibolites. Composition 4/7 corresponds to phlogopite that seems to be a retrograde product of edenite (anal. 4/5).

#### Scapolite

This mineral is part of the younger paragenesis in the metabasic rocks from Cóbdar and has not been found in the Lugros suite (Table 5). It is particularly abundant in the Cóbdar metabasalts overlain by the evaporitic metasediments of the Soportújar Formation (Puga *et al.* 1996). The marialite content in this scapolite is about 75 mol.% (Portugal *et al.* 1987).

#### Feldspars

Albite containing less than 5% An is common in symplectitic intergrowths with amphibole, replacing omphacite, or as poikiloblasts with inclusions of calcic or sodic-calcic amphibole, epidote and mica from both the Cóbdar and Lugros metabasic rocks. Composition 2/6 corresponds to albite in equilibrium with edenite (anal. 2/5) in a metapillow from Cóbdar, whereas compositions 4/2 and 4/3 refer to an albite–taramite pair from the Lugros eclogites. The relics of igneous plagioclase in some samples from Cóbdar correspond to a twinned labradorite, with an An content from 60 to 70 mol.%, increasing toward the rim (Figs. 3a, b).

#### Kyanite

This mineral is relatively abundant in the metabasic rocks from Lugros; in contrast, it is absent in those from the Cóbdar suite, although there is no bulk chemical control justifying this mineralogical difference (Puga *et al.* 1989a, 1995). In the pillows, kyanite replaces fibrous aggregates of clinozoisite, locally associated with para-

gonite, which replaces plagioclase microphenocrysts. In this texture, kyanite is associated with omphacite and garnet. Kyanite also fills veinlets a few millimeters thick, locally associated with omphacite (Fig. 4b), cross-cutting the garnet–omphacite eclogitic assemblage. In some metabasalts, kyanite was formed in association with omphacite at the climax of the eo-Alpine metamorphic event, and it is partially replaced by paragonite (Fig. 4d).

#### Rutile

Rutile is an accessory phase, albeit ubiquitous, in these metabasic rocks. It appears as random crystals in the matrix or as inclusions in poikiloblasts of various metamorphic phases. In some metadiabases and metagabbros, it seems to have formed from primary ilmenite. It is particularly abundant as very small inclusions in the omphacite that replaces igneous augite during the eclogitic stage, and in the amphiboles replacing this omphacite in the subsequent amphibolite stage.

#### Quartz

Quartz is a minor phase present in some of the metabasic rocks from Cóbдар and Lugros. It appears in the matrix of these rocks, as inclusions in the garnet of eclogites, and in the pressure shadows of these minerals, locally associated with omphacite.

#### ESTIMATION OF THE P–T METAMORPHIC CONDITIONS

Figure 10 summarizes the estimated P–T conditions of evolution for the Cóbдар and Lugros metabasic rocks. Inferences about the physical conditions that prevailed during each of the successive stages of blastesis are based on experimental phase-equilibria curves for metabasic rocks, conventional thermobarometric methods and, wherever possible, multi-equilibrium calculations. The succession of stages of blastesis established (Table 5) is based on the zoning patterns of garnet, pyroxene and amphibole, as well as the textural relations described in the above sections. Although Figures 3 and 4 have been selected to show the textural and mineralogical evolution of the basic rocks from Cóbдар and Lugros, from the igneous paragenesis to the successive metamorphic assemblages, all the thermobarometric estimates were done in domains of samples showing textural and chemical evidence of equilibrium among the phases under consideration.

The available information about the P–T conditions of the metamorphic mineral phases and associations present in Cóbдар and Lugros meta-ophiolites have been plotted in Figure 10. Reactions plotted in this figure are known with various degrees of certainty. Qualitative information about the stability field of some mineral phases can be obtained from the reactions  $Lws/Ab + Jd = Zo + Pg + Qtz$  (Holland 1979b, Ghent *et al.* 1993),  $Pl$

$= Pg + Zo$  (Franz & Althaus 1977) and the  $Gln = Act$  transition (Maruyama *et al.* 1986). Semiquantitative information in this P–T space can be obtained with the graphical geobarometer of Massonne & Schreyer (1987), which allows us to estimate minimum pressures given the absence of biotite and K-feldspar in the paragenesis. Finally, quantitative estimates of P–T include: 1) the jadeite content of clinopyroxene in equilibrium with kyanite and paragonite (assuming an  $H_2O$  activity of 1, as expected in this type of mineral assemblages, similar to those described from the Tauern eclogites by Holland (1979a), 2) the garnet–omphacite geothermometer of Ellis & Green (1979), 3) the THERMOCALC determinations, and 4) the plagioclase–amphibole geothermometer of Holland & Blundy (1994).

#### The eo-Alpine event

The estimated P–T conditions of the eo-Alpine episode of metamorphism for the Cóbдар and Lugros rocks (dark and light gray, respectively, in the upper part of Fig. 10) can be constrained by the absence of lawsonite, the garnet–omphacite equilibria, the jadeite content in omphacite, and the coexistence, or not, of kyanite and paragonite in equilibrium with omphacite.

In the Cóbдар suite, information about prograde metamorphic assemblages prior to the peak pressure of the eclogite facies is tentatively provided by the presence, in some rocks without penetrative deformation of palmate aggregates of clinozoisite + paragonite replacing plagioclase phenocrysts, which might have been previously transformed into lawsonite and albite judging from the occasional preservation of albite remains in these microdomains. The slope of the initial part of the prograde path, prior to intersection with the  $Lws + Ab = Zo + Pg + Qtz$  reaction (which would lead to the palmate pseudomorphs of the igneous plagioclase) might be similar to the P–T evolution experienced by a 50-Ma-old oceanic slab during subduction (Peacock 1990), taking into account the most probable ages of magmatism and eo-Alpine metamorphism deduced for the Betic Ophiolitic Association (Portugal *et al.* 1988, Puga *et al.* 1991, 1995, Nieto *et al.* 1997b).

The eo-Alpine metamorphic climax in the Cóbдар suite was probably close to conditions at the boundary between glaucophane-schist and eclogite facies, considering the scarce development of eclogitic parageneses in these rocks. Two types of coexisting high-pressure assemblages can be found in the Cóbдар region in metabasic rocks with similar bulk chemical composition. The first type is  $Gln + Czo + Pg + Omp + Qtz \pm Grt$ , with a jadeite content in the omphacite of 45 to 50 mol.%. Compositions 1/16 and 1/17 in Table 1 correspond, respectively, to omphacite and glaucophane from these rocks. The other high-pressure assemblage comprises  $Alm + Omp + Rt + Qtz$ , with a jadeite content in omphacite of 39 to 44 mol.%. Temperatures obtained

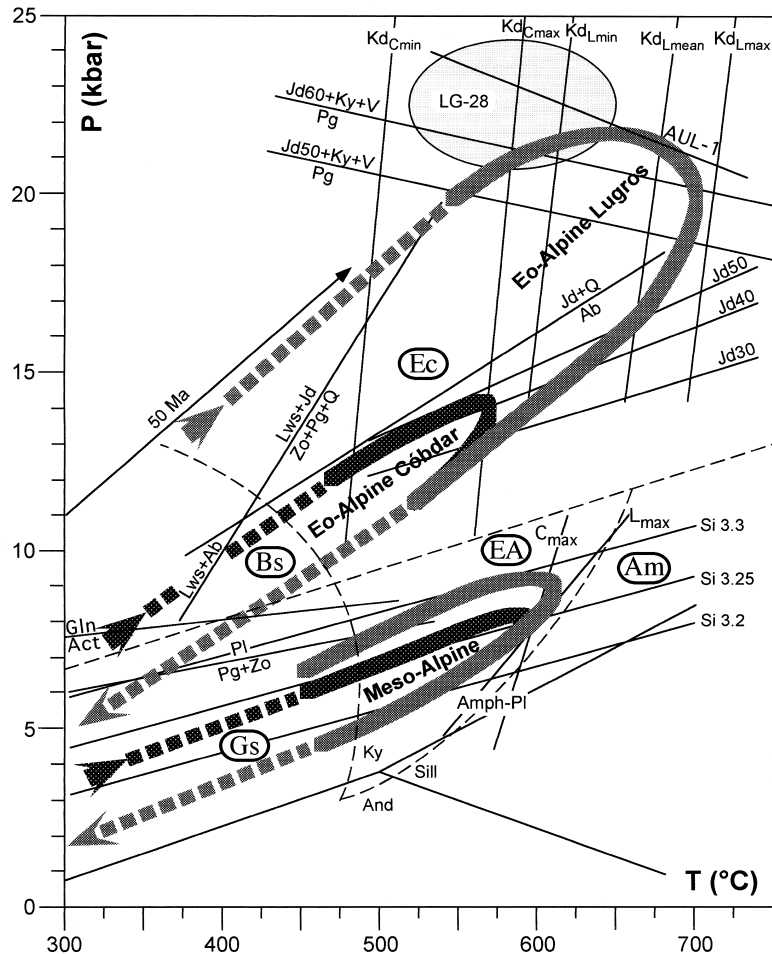


FIG. 10. P-T diagram showing the estimated conditions of prograde and retrograde metamorphism during the formation of the eclogitic and amphibolitic parageneses of the Cóbдар (dark gray path) and Lugros (light grey path) metabasic rocks. Maximum and minimum estimates of temperature for the eclogitic parageneses in Cóbдар ( $K_{dC}$ ) and Lugros ( $K_{dL}$ ) were calculated using  $K_d$  values of garnet-clinopyroxene pairs (Ellis & Green 1979), whereas the maximum temperatures for the amphibolite stage in Cóbдар ( $C_{max}$ ) and Lugros ( $L_{max}$ ) were obtained with plagioclase-amphibole pairs according to Holland & Blundy (1994). The line defined with the eclogitic assemblage in sample AUL-1 and the field defined with the assemblage in sample LG-28 were calculated using THERMOCALC (Powell & Holland 1988). For the Cóbдар metabasic rocks, the prograde path of the amphibole stage has been plotted, although discontinuously, starting from surface conditions to accommodate geological evidence (Puga *et al.* 1996). Reactions plotted in the figure are:  $Jd + Ky + V = Pg$  (Holland 1979a);  $Lw + Jd = Zo + Pg + Qtz$  (Holland 1979b);  $Ab + Jd = Zo + Pg + Qtz$  (Holland 1979b);  $Pl = Pg + Zo$  (Franz & Althaus 1977). Also shown are isopleths of jadeite content in omphacite (Gasparik & Lindsley 1980), Si content (*apfu*) of phengite (Massone & Schreyer 1987), the lower stability limit of glaucophane after Maruyama *et al.* (1986), and the  $Al_2O_3$  triple point according to Holdaway (1971). Also plotted in the diagram is a model P-T path for a 50-Ma subducted oceanic crust after Peacock (1990). The boundaries between metamorphic facies, in dashed lines, are shown for reference and are those of Spear (1993). Ec: eclogite facies, Bs: blueschist facies, Gs: greenschist facies, Am: amphibolite facies, EA: albite-epidote amphibolite facies.

using the geothermometer of Ellis & Green (1979), with garnet–omphacite pairs in contact and without evidence of retrogression, range from 480°C (anal. 1/12 and 1/13), with  $K_{d\text{ Fe-Mg}} = 32.62$ ,  $X_{\text{Ca}}$  in garnet = 0.295 and 39.6 mol.% of jadeite in omphacite, to 570°C (anal. 1/14 and 1/15), with  $K_{d\text{ Fe-Mg}} = 20.49$ ,  $X_{\text{Ca}}$  in garnet = 0.31 and 44 mol.% jadeite in omphacite. Therefore, the P–T conditions of equilibration during the high-pressure event in this suite can be estimated at 480 to 570°C and 12.5 to 14.2 kbar, although the fact that the lower temperatures are obtained in garnet–omphacite core pairs with a low jadeite content suggests that these pairs could represent the final part of the prograde path toward climax conditions.

The retrograde eo-Alpine trajectory in the Córdar metabasic rocks is not well constrained and can only be inferred from the formation of glaucophane and amphibole–albite symplectite, after omphacite, and, in some rocks, from the replacement of igneous plagioclase relics by paragonite-rich white mica and clinozoisite according to the reaction  $\text{Pl} = \text{Pg} + \text{Zo}$ . During the intermediate pressure (IP) amphibolite stage, the white mica aggregates, derived from plagioclase, were replaced at their rim by albite and barroisite poikiloblasts, whereas the clinozoisite was overgrown by epidote with a higher Fe content.

The eo-Alpine prograde path reached higher P–T conditions in the Lugros metabasic rocks than in the ones from Córdar (Fig. 10). The first prograde orogenic assemblage in the Lugros suite is clinozoisite + paragonite in palmate aggregates that replace plagioclase phenocrysts in conditions most probably corresponding to the reaction  $\text{Lws} + \text{Jd} = \text{Zo} + \text{Pg} + \text{Qtz}$ . This reaction may represent the final product of high-pressure breakdown of plagioclase during the prograde metamorphism toward the peak eclogitic conditions. The slope of the initial part of the prograde path has been plotted, as for the Córdar one, for the same reasons as explained above.

The peak eclogitic assemblage in this suite consists of  $\text{Alm} + \text{Omp} + \text{Ky} + \text{Pg} + \text{Czo} + \text{Rt} + \text{Qtz}$ , with a jadeite content in omphacite varying from 45 to 64 mol.%. The temperature range for this assemblage falls between the curves  $K_{d\text{ Lmin}}$  and  $K_{d\text{ Lmax}}$  in Figure 10, representing the extreme  $K_{d\text{ Fe-Mg}}$  values of omphacite–garnet pairs obtained with the geothermometer of Ellis & Green (1979).  $K_{d\text{ Lmin}} = 9.75$ , for  $X_{\text{Ca}}$  in garnet = 0.143, corresponds to compositions 3/2 and 3/3, and  $K_{d\text{ Lmax}} = 7.45$ , for  $X_{\text{Ca}}$  in garnet = 0.145, corresponds to compositions 3/4 and 3/5. The pressure range for the peak assemblage is inferred from the equilibrium  $\text{Pg} = \text{Jd}_{45-64} + \text{Ky} + \text{V}$  (Holland 1979b), corresponding to about 20–22 kbar at 600 to 700°C (Fig. 10), assuming an  $\text{H}_2\text{O}$  activity of 1, as expected in this type of mineral assemblage (Holland 1979a).

Glaucophane in the Lugros metabasic rocks occupies the same textural positions as in the ones from Córdar; it forms inclusions in garnet poikiloblasts, mainly

formed during the prograde eo-Alpine stage, but more commonly, it is found as a replacement of omphacite, taking place during the retrograde eo-Alpine stage. However, in some rock types richer in Na and Fe, glaucophane crystals also seem to be coeval with omphacite and almandine, and formed under peak conditions (Fig. 4d). In these samples, the texturally retrograde crystals of glaucophane (anal. 3/12) are transformed toward their margin to taramite (anal. 4/2) with notably lower  $\text{Na}^{\text{M4}}$ , fAl and  $\text{Na}/(\text{Na} + \text{Ca})$  values, and higher  $^{\text{IV}}\text{Al}$  and  $\text{Al}/(\text{Al} + \text{Si})$  values (Figs. 4d, 8, 9), suggesting a notable shift in the conditions toward lower P and higher T. This abrupt change in physical conditions does not seem to correspond to a gradual, prograde or retrograde evolution during the same event but, more probably, to two periods of blastesis corresponding to different metamorphic events. This is why taramite and other Na–Ca amphiboles, which originated as products of transformation of the eclogitic paragenesis in the BOA metabasic rocks, have been attributed to the subsequent meso-Alpine event (Table 5).

In order to obtain additional information on the pressure and temperature conditions of equilibration of the high-pressure assemblages in the Córdar and Lugros suites, we used the average P–T method of Powell & Holland (1994) with the computer program THERMOCALC (Powell & Holland 1988, version 2.6) and the internally consistent thermodynamic dataset of Hol-

TABLE 6a. RESULTS OF CALCULATIONS OF AVERAGE P–T CONDITIONS FROM THE HIGH-PRESSURE ASSEMBLAGE IN SAMPLE AUL-1 USING THERMOCALC VERSION 2.6\*

|                   | Prp     | Grs     | Alm     | Pg      | Mrg              | Czo     | Di      |
|-------------------|---------|---------|---------|---------|------------------|---------|---------|
| Activity(a):      | 0.0230  | 0.0270  | 0.100   | 0.730   | 0.0176           | 0.230   | 0.400   |
| $\sigma(\ln a)$ : | 0.46089 | 0.44100 | 0.25841 | 0.15000 | 0.56818          | 0.17787 | 0.10800 |
|                   | Hd      | Jd      | Ky      | Qtz     | H <sub>2</sub> O |         |         |
| Activity(a):      | 0.0840  | 0.510   | 1.00    | 1.00    | 1.00             |         |         |
| $\sigma(\ln a)$ : | 0.30261 | 0.10000 | 0       | 0       |                  |         |         |

Incomplete independent set of reactions

- 1)  $\text{Pg} = \text{Jd} + \text{Ky} + \text{H}_2\text{O}$
- 2)  $2\text{Pg} + 3\text{Hd} = \text{Grs} + \text{Alm} + 2\text{Jd} + 2\text{Qtz} + 2\text{H}_2\text{O}$
- 3)  $13\text{Pg} + 12\text{Hd} = 4\text{Alm} + 6\text{Czo} + 13\text{Jd} + 7\text{Qtz} + 10\text{H}_2\text{O}$

Calculations for the independent set of reactions

|   | P(T) | sd(P) | a      | sd(a) | b        | c       | ln K   | sd(ln K) |
|---|------|-------|--------|-------|----------|---------|--------|----------|
| 1 | 23.0 | 0.82  | 37.96  | 0.34  | -0.01336 | -1.050  | -0.359 | 0.112    |
| 2 | 22.5 | 2.70  | 72.63  | 1.55  | -0.01696 | -2.846  | 0.799  | 1.066    |
| 3 | 20.7 | 2.22  | 311.93 | 7.74  | -0.09156 | -13.740 | 7.033  | 4.184    |

Average pressures [for  $X(\text{H}_2\text{O}) = 1.0$ ]

| T°C         | 450  | 500  | 550  | 600  | 650  | 700  |
|-------------|------|------|------|------|------|------|
| av P        | 25.5 | 24.6 | 23.6 | 22.7 | 21.8 | 21.0 |
| $\sigma(P)$ | 1.45 | 1.33 | 1.19 | 1.03 | 0.87 | 0.92 |
| sigfit      | 2.1  | 1.8  | 1.5  | 1.2  | 1.0  | 0.8  |

\* dataset of April 1996.

TABLE 6b. RESULTS OF CALCULATIONS OF AVERAGE P-T CONDITIONS FROM THE HIGH-PRESSURE ASSEMBLAGE IN SAMPLE LG-28 USING THERMOCALC VERSION 2.6\*

|                   | Prp     | Grs     | Alm     | Pg      | Mrg     | Gln     | Fgln    |
|-------------------|---------|---------|---------|---------|---------|---------|---------|
| Activity(a):      | 0.00920 | 0.00760 | 0.200   | 0.860   | 0.0233  | 0.0790  | 0.0490  |
| $\alpha(\ln a)$ : | 0.56235 | 0.58089 | 0.15515 | 0.10000 | 0.42918 | 0.31012 | 0.36377 |

|                   | Rbk     | Czo     | Ep      | Di      | Hd      | Jd      | Ae      |
|-------------------|---------|---------|---------|---------|---------|---------|---------|
| Activity(a):      | 0.00262 | 0.220   | 0.720   | 0.230   | 0.0370  | 0.500   | 0.230   |
| $\alpha(\ln a)$ : | 0.66896 | 0.18252 | 0.10000 | 0.17787 | 0.39138 | 0.10000 | 0.17787 |

|                   | Ky   | Qtz  | H <sub>2</sub> O |
|-------------------|------|------|------------------|
| Activity(a):      | 1.00 | 1.00 | 1.00             |
| $\alpha(\ln a)$ : | 0    | 0    |                  |

## Independent set of reactions

- 1) Mrg + 4 Czo = 3 Grs + 5 Ky + 3 H<sub>2</sub>O
- 2) 3 Mrg + 2 Qtz = Grs + 5 Ky + 3 H<sub>2</sub>O
- 3) Pg = Jd + Ky + H<sub>2</sub>O
- 4) Pg + Gln = Prp + 3 Jd + 2 Qtz + 2 H<sub>2</sub>O
- 5) 7 Grs + 12 Pg + 3 Di = Prp + 12 Czo + 12 Jd + 6 H<sub>2</sub>O
- 6) Grs + 13 Mrg + 5 Fgln = 5 Alm + 10 Pg + 8 Czo + 4 H<sub>2</sub>O
- 7) 2 Pg + Rbk = Fgln + 2 Ae + 2 Ky + 2 H<sub>2</sub>O
- 8) 4 Grs + Alm + 4 Pg + 2 Ep + 3 Qtz = Fgln + 8 Czo + 2 Ae
- 9) Pg + Ep + 3 Hd + Ae = Grs + Rbk + Czo

## Calculations for the independent set of reactions

|   | P(T) | sd(P) | a      | sd(a) | b        | c      | ln K   | sd(ln K) |
|---|------|-------|--------|-------|----------|--------|--------|----------|
| 1 | 22.1 | 4.35  | 142.13 | 1.66  | -0.03596 | -3.344 | -4.823 | 1.938    |
| 2 | 28.1 | 2.59  | 68.92  | 0.69  | -0.00152 | -4.073 | 6.398  | 1.413    |
| 3 | 20.8 | 1.06  | 36.73  | 0.34  | -0.01211 | -1.050 | -0.542 | 0.141    |
| 4 | 22.3 | 2.76  | 159.38 | 1.02  | -0.09468 | -1.970 | -4.079 | 0.716    |
| 5 | 22.1 | 5.35  | 131.92 | 6.33  | -0.05001 | -7.053 | 9.200  | 4.981    |
| 6 | 29.8 | 5.39  | 94.04  | 23.04 | -0.17545 | -9.604 | 47.162 | 6.206    |
| 7 | 28.9 | 3.60  | 92.16  | 4.63  | -0.03401 | -2.205 | 0.291  | 0.864    |
| 8 | 25.8 | 87.78 | -95.99 | 10.80 | 0.06330  | 0.270  | 4.320  | 2.831    |
| 9 | 15.3 | 39.14 | -57.01 | 4.96  | 0.07273  | -0.313 | -0.499 | 1.499    |

Average P-T conditions [for  $X(\text{H}_2\text{O}) = 1.0$ ]

T = 585°C, sd = 67,  
P = 22.7 kbar, sd = 2.1, cor = -0.496, sigfit = 2.02

\* dataset of April 1996. The IMA-approved symbol Ae has been substituted for Acn (acmite, now discredited).

land & Powell (1990, dataset April 1996). End-member activities were calculated using the computer program AX (version 2.2) and the defaults suggested by Powell & Holland (1988).

In the Córdar eclogites, it was not possible to find an independent set of reactions among the end-members of the minerals in the high-pressure assemblage. In the case of the Lugros eclogites, we calculated the average P-T conditions of two high-pressure mineral assemblages from two samples with different bulk chemical compositions (Tables 6a, 6b). In both cases, an H<sub>2</sub>O activity of 1 has been used, although the results are similar if we use a mixture of H<sub>2</sub>O with CO<sub>2</sub> or any other ideal solution with at least 80% H<sub>2</sub>O, as has been deduced for a similar type of mineral assemblage (Holland 1979a). In sample AUL-1, the assemblage Grt + Omph + Pa + Ky + Czo + Qtz + H<sub>2</sub>O yields an average P = 22.7 ± 1.03 kbar for T = 600°C, and P = 21.0 kbar ±

TABLE 6c. CHEMICAL COMPOSITION OF MINERAL PHASES IN SAMPLES AUL-1 AND LG-28\*

|                                | AUL-1  |       |       |        | LG-28 |       |       |       |       |
|--------------------------------|--------|-------|-------|--------|-------|-------|-------|-------|-------|
|                                | Grt    | Ms    | Ep    | Cpx    | Grt   | Ms    | Amp   | Ep    | Cpx   |
| SiO <sub>2</sub> wt%           | 38.52  | 47.38 | 36.22 | 56.73  | 36.04 | 46.05 | 55.50 | 36.85 | 54.06 |
| TiO <sub>2</sub>               | 0.15   | 0.24  | 0.04  | 0.03   | 0.22  | 0.05  | 0.03  | 0.13  | 0.07  |
| Al <sub>2</sub> O <sub>3</sub> | 21.91  | 37.97 | 22.96 | 12.31  | 21.09 | 39.08 | 9.40  | 23.26 | 12.50 |
| Cr <sub>2</sub> O <sub>3</sub> | 0.06   | 0.00  | 0.04  | 0.05   | 0.05  | 0.00  | 0.00  | 0.00  | 0.00  |
| Fe <sub>2</sub> O <sub>3</sub> | 1.10   | 0.00  | 13.49 | 0.37   | 3.91  | 0.00  | 3.06  | 13.96 | 8.45  |
| FeO                            | 22.74  | 0.90  | 0.54  | 2.94   | 27.40 | 0.76  | 10.21 | 0.13  | 1.28  |
| MnO                            | 0.93   | 0.02  | 0.08  | 0.01   | 0.52  | 0.00  | 0.00  | 0.11  | 0.02  |
| MgO                            | 5.71   | 0.72  | 0.01  | 7.80   | 4.17  | 0.09  | 10.35 | 0.03  | 4.56  |
| CaO                            | 9.45   | 0.20  | 23.35 | 12.16  | 6.12  | 0.22  | 0.74  | 23.27 | 7.46  |
| Na <sub>2</sub> O              | 0.05   | 6.21  | 0.01  | 7.64   | 0.02  | 7.04  | 7.02  | 0.00  | 9.86  |
| K <sub>2</sub> O               | 0.00   | 2.39  | 0.00  | 0.00   | 0.00  | 0.79  | 0.01  | 0.00  | 0.00  |
| Total                          | 100.62 | 96.03 | 96.74 | 100.06 | 99.54 | 94.08 | 96.32 | 97.76 | 98.27 |

Quartz and kyanite not included.

0.92 kbar for T = 700°C. These results are consistent with the P-T estimates previously discussed for the Lugros eclogites using conventional thermobarometric methods, and have been represented as curve AUL-1 in Figure 10. Sample LG-28 has a bulk chemical composition slightly different from the rest of the eclogites studied from the Lugros suite, with lower Ca and higher Na and Fe contents. In this sample, occasional glaucophane and omphacite crystals appear as inclusions near the rim of the poikiloblastic garnet. Therefore, we assumed that the inclusions of glaucophane and omphacite in the poikiloblastic garnet in this sample could have formed during the prograde eo-Alpine path, near the climax conditions. To calculate average P-T conditions for this assemblage, we carefully selected a domain where all the minerals of the peak assemblage were next to each other and in apparent textural equilibrium, and where the glaucophane inclusions were as close as possible to the garnet rim (Fig. 4c). The assemblage yielded an average T of 585 ± 67°C and an average P of 22.7 ± 2.1 kbar (95% confidence level in both cases), represented in Figure 10 by the ellipse labeled LG-28. These results are also consistent with the previous estimates, especially if we consider that glaucophane could be a prograde phase near the peak conditions.

### The meso-Alpine event

Pressure conditions during the meso-Alpine event were estimated using the Si content of phengitic micas (Massone & Schreyer 1987), the lower stability limit of glaucophane after Maruyama *et al.* (1986) for the limiting reactions between the blueschist and greenschist facies, and the Al<sub>2</sub>O<sub>3</sub> triple point of Holdaway (1971). Peak conditions of temperature were determined using the plagioclase-amphibole geothermometer of Holland

& Blundy (1994). As no further quantitative or semiquantitative data were available, the correlations between  $^{IV}Al$  and T (Brown 1977), and between the  $Na^{M4}$  and fAl values and P (Brown 1977, Smith 1988) in amphiboles, were also taken into account in a very qualitative way.

In the *Cóbdar* metabasic rocks, meso-Alpine peak conditions are constrained by the association of phengitic mica, Na–Ca amphibole and albite. Temperature estimates for this assemblage in various samples, made using the plagioclase–amphibole geothermometer of Holland & Blundy (1994), provide maximum values of around 580°C at 6 kbar and 615°C at 10 kbar (Fig. 10), as is the case of the edenite (anal. 2/5) and albite (anal. 2/6) pair represented in Table 2. Phengite in this assemblage has a Si content of around 3 *apfu*, and up to 3.22 *apfu* (anal. 2/4). As this phengite is not coeval with biotite and K-feldspar, minimum pressures can be estimated at around 8 kbar (Massonne & Schreyer 1987).

The P–T conditions of the meso-Alpine event in the metabasic rocks from *Lugros* are similar to those from *Cóbdar* (Fig. 10). Nonetheless, Figure 8 suggests that most of the *Lugros* amphiboles formed at higher P (higher  $Na^{M4}$  values) than those from *Cóbdar*, although at a similar T (similar  $^{IV}Al$  values). Moreover, the plot of  $Na/(Na + Ca)$  versus  $Al/(Al + Si)$  of these amphiboles in Figure 9 points to a higher metamorphic gradient for *Cóbdar* than for *Lugros* amphiboles. These chemical differences in Na–Ca amphiboles justify the slightly different prograde meso-Alpine paths represented for the *Cóbdar* and *Lugros* metabasic rocks in Figure 10.

The metabasic rocks from *Lugros* equilibrated during the meso-Alpine climax at maximum temperatures of around 560°C at 6 kbar and 665°C at 10 kbar, according to the plagioclase–amphibole geothermometer of Holland & Blundy (1994) applied to the taramite–albite pair 4/2 and 4/3 in Table 4. Phengite in this assemblage, with a Si content of about 3.3 *apfu*, indicates an equilibration P above 9 kbar. Therefore, although the P–T conditions during the meso-Alpine event seem to be similar for both suites (8–9 kbar, 575–625°C), a slightly higher P of equilibration for the same T can be deduced for the *Lugros* rocks. The meso-Alpine retrograde path for the *Lugros* and *Cóbdar* suites most probably took place under the same P–T conditions, considering the similar composition of the retrograde minerals in both suites, especially the composition of the edenite (Fig. 10) that rims barroisite or taramite crystals (Figs. 8, 9).

#### CONCLUDING REMARKS

Metabasic rocks of dismembered meta-ophiolitic suites at *Lugros* and *Cóbdar* present evidence of a plurifacial Alpine metamorphic evolution that largely overprinted the igneous and ocean-floor metamorphic assemblages of Jurassic age (Puga *et al.* 1989a, 1995). The Alpine orogenic metamorphism in these rocks was

characterized by two main metamorphic events: 1) the eo-Alpine, which developed assemblages of the kyanite-bearing eclogite facies in *Lugros*, and glaucophane schists to eclogite facies in *Cóbdar*, in both cases followed by a retrograde stage in P–T conditions typical of glaucophane schist; 2) the subsequent, and more penetrative meso-Alpine event, which formed albite–epidote amphibolite facies, partially retrograded to greenschists in both suites.

The eo-Alpine and meso-Alpine metamorphic events in these metabasic rocks most probably developed during the Late Cretaceous – Paleocene and Late Eocene – Oligocene, respectively, taking into account the available petrological, geological and geochronological lines of evidence reviewed earlier. These two metamorphic events in the *Mulhacén* Complex may be related with two periods of convergence of the Iberian and African Plates, separated by a period of relaxation during the Paleocene and Early Eocene (Dewey *et al.* 1989), during which the *Soportújar* Formation was deposited onto the eclogitized and exhumed ophiolites and over other units of the *Mulhacén* Complex (Puga *et al.* 1996).

Different P–T conditions of equilibration were attained during the eo-Alpine event in the *Cóbdar* (480–570°C and 12.5–14.2 kbar) and *Lugros* suites (600–700°C and 21–22 kbar). These differences have been also recognized among other exposures of ophiolitic units from the eastern and western parts of the BOA, and suggest the existence of an eo-Alpine metamorphic gradient with increasing P–T conditions toward the west in the *Mulhacén* Complex (Fig. 1). This increase in P–T conditions of eo-Alpine metamorphism might reflect a westward-dipping subduction of the oceanic slab from which these ophiolites were derived, as well as of its continental margins. A probable westward subduction of the Betic units had been suggested as a result of the accommodation of the movement of Iberia toward the east-southeast due to the opening of the North Atlantic and the Bay of Biscay during the Cretaceous (De Jong 1991, Zeck 1996). Moreover, recent tomographic images of the mantle below the Betic Cordillera (Blanco & Sparkman 1993, Blanco 1995) show the presence of a SW–NE-striking lithospheric slab with a small NW-dipping component, also pointing to a westward-dipping subduction of the detached slab. An eo-Alpine high-pressure metamorphic gradient, increasing toward the geosuture zone, has traditionally been accepted for different parts of the Alpine belt (Ernst 1973, Frey *et al.* 1974). However, until now, a proposal based on petrological evidence had not been formulated for the Betic Cordillera.

The preservation of relics of the igneous paragenesis in some samples from *Cóbdar* contrasts with the situation in the *Lugros* and other ophiolite suites from *Sierra Nevada* (Fig. 1), where only igneous textures and structures have been preserved. There are several causes that could explain the preservation of igneous parageneses in the *Cóbdar* metabasic rocks, such as the lower

P-T conditions attained, and the shorter time-period during which these rocks were subducted. Given the scarce development of the eo-Alpine parageneses in the C6bdar area, the most plausible working hypothesis seems to be that the time span during which the rocks were under glaucophane schist to eclogitic conditions was not sufficient for them to completely attain equilibrium.

The conditions of meso-Alpine metamorphism were very similar in both the C6bdar and Lugros metabasic rocks, with peak conditions of about  $600 \pm 25^\circ\text{C}$  and  $8.5 \pm 0.5$  kbar, although the prograde metamorphic conditions are slightly different in the two localities, as suggested by the composition of the amphiboles generated from the pre-existing eclogite and glaucophane-schist parageneses. This metamorphic event most probably developed during a Late Eocene – Oligocene collisional stage of the Betic Orogen and was related to the stacking of the Betic Complexes and the development of the most penetrative regional foliation in all the Betic units. Finally, during the Late Oligocene – Miocene, there was an important phase of exhumation and cooling of the metamorphic rocks accompanied by minor metamorphic recrystallization, mainly along extensional tectonic contacts.

#### ACKNOWLEDGEMENTS

The authors are indebted to L. Aguirre (Santiago de Chile), A. Demant (Marseille), E.D. Ghent (Calgary), A. Indares (St. John's, Newfoundland), P. Monié (Montpellier), P.J. O'Brien (Bayreuth) and R.F. Martin (Montreal) for critical reviews, which greatly improved the manuscript. Financial support from Spanish Project PB 95-0220 and from the Research Group of the Junta de Andalucía RMN187 is acknowledged.

#### REFERENCES

- ANDRIESEN, P.A.M., HEBEDA, E.H., SIMON, O.J. & VERSCHURE, R.H. (1991): Tourmaline K–Ar ages compared to other radiometric dating systems in Alpine anatectic leucosomes and metamorphic rocks (Cyclades and southern Spain). *Chem. Geol.* **91**, 33-48.
- BAKKER, H.E., DE JONG, K., HELMERS, H. & BIERMANN, C. (1989): The geodynamic evolution of the Internal Zone of the Betic Cordilleras (south-east Spain): a model based on structural analysis and geothermobarometry. *J. Metamorph. Geol.* **7**, 359-381.
- BLANCO, M.J. (1995): *Tomografía lineal con residuos temporales del manto bajo la Península Ibérica*. Tesis doctoral, Universidad Complutense de Madrid, Madrid, Spain.
- \_\_\_\_\_ & SPARKMAN, W. (1993): The P-wave velocity structure of the mantle below the Iberian Peninsula: evidence for subducted lithosphere below southern Spain. *Tectonophys.* **221**, 13-34.
- BODINIER, J.-L., MORTEN, L., PUGA, E. & DÍAZ DE FEDERICO, A. (1987): Geochemistry of metabasites from the Nevado-Filábride Complex, Betic Cordilleras, Spain: relicts of a dismembered ophiolitic sequence. *Lithos* **20**, 235-245.
- BROWN, E.H. (1977): The crossite content of Ca-amphibole as a guide to pressure of metamorphism. *J. Petrol.* **18**, 53-72.
- CÁMARA, F. (1995): *Estudio cristalquímico de minerales metamórficos en rocas básicas del Complejo Nevado-Filábride (Cordilleras Béticas)*. Tesis doctoral, Univ. Granada, Granada, Spain.
- CARPENTER, M.A. (1979): Omphacites from Greece, Turkey, and Guatemala: composition limits of cation ordering. *Am. Mineral.* **64**, 102-108.
- CAWTHORN, R.G. & COLLERSON, K.D. (1974): The recalculation of pyroxene end-member parameters and the estimation of ferrous and ferric iron content from electron microprobe analyses. *Am. Mineral.* **59**, 1203-1208.
- DE JONG, K. (1991): *Tectono-Metamorphic Studies and Radiometric Dating in the Betic Cordilleras (SE Spain)*. Ph.D. thesis, Vrije Universiteit, Amsterdam, The Netherlands.
- DESMONS, J. (1989): Different metamorphic evolutions in the Alpine-Apenninic ophiolites (France – Italy – Switzerland – Austria). *Chem. Geol.* **77**, 229-250.
- DEWEY, J.F., HELMAN, M.L., TURCO, E., HUTTON, D.H.W. & KNOTT, S.D. (1989): Kinematics of the western Mediterranean. In *Alpine Tectonics* (M. Coward, D. Dietrich & R.G. Park, eds.). *Geol. Soc., Spec. Publ.* **45**, 265-283.
- DÍAZ DE FEDERICO, A. (1980): *Estudio geológico del Complejo de Sierra Nevada en la Transversal del Puerto de la Ragua (Cordillera Bética)*. Tesis doctoral, Univ. Granada, Granada, Spain.
- \_\_\_\_\_, TORRES ROLDÁN, R.L. & PUGA, E. (1990): The rock series of the Betic Substratum. In *Les Basins Néogènes du Domaine Bélique Oriental (Espagne)*. *Documents et Travaux IGAL (Paris)* **12-13**, 19-29.
- DIETRICH, V. (1980): The distribution of ophiolites in the Alps. *Ophioliti, Spec. Issue* **1**, 7-51.
- DROOP, G.T.R. (1987): A general equation for estimating Fe<sup>3+</sup> concentrations in ferromagnesian silicates and oxides from microprobe analyses, using stoichiometric criteria. *Mineral. Mag.* **51**, 431-435.
- ELLIS, D.J. & GREEN, D.H. (1979): An experimental study of the effect of Ca upon garnet-clinopyroxene Fe–Mg exchange equilibria. *Contrib. Mineral. Petrol.* **71**, 13-22.
- ERNST, W.G. (1973): Interpretative synthesis of metamorphism in the Alps. *Geol. Soc. Am., Bull.* **84**, 2053-2078.
- FRANZ, G. & ALTHAUS, E. (1977): The stability relations of the paragenesis paragonite – zoisite – quartz. *Neues Jahrb. Mineral., Abh.* **130**, 159-167.

- FREY, M., HUNZIKER, J.C., FRANK, W., BOCQUET, J., DAL PIAZ, G.V., JÄGER, E. & NIGGLI, E. (1974): Alpine metamorphism of the Alps. A review. *Schweiz. Mineral. Petrogr. Mitt.* **54**, 247-290.
- GASPARIK, T. & LINDSLEY, D.H. (1980): Phase equilibria at high pressures of pyroxenes containing monovalent and trivalent ions. In *Pyroxenes* (C.T. Prewitt, ed.). *Rev. Mineral.* **7**, 309-339.
- GHEENT, E.D., STOUT, M.Z. & ERDMER, P. (1993): Pressure-temperature evolution of lawsonite-bearing eclogites, Pinchi Lake, British Columbia. *J. Metamorph. Geol.* **11**, 279-290.
- GÓMEZ-PUGNAIRE, M.T. & FERNÁNDEZ-SOLER, J.M. (1987): High-pressure metamorphism in metabasites from the Betic Cordilleras (SE Spain) and its evolution during the Alpine orogeny. *Contrib. Mineral. Petrol.* **95**, 231-244.
- HEBEDA, E.H., BOELRIJK, N.A.I.M., PRIEM, H.N.A., VERDURMEN, E.A.T., VERSCHURE, R.H. & SIMON, O.J. (1980): Excess radiogenic Ar and undisturbed Rb-Sr systems in basic intrusives subjected to Alpine metamorphism in southeastern Spain. *Earth Planet. Sci. Lett.* **47**, 81-90.
- HOLDAWAY, M.J. (1971): Stability of andalusite and the aluminum silicate phase diagram. *Am. J. Sci.* **271**, 97-131.
- HOLLAND, T.J.B. (1979a): High water activities in the generation of high pressure kyanite eclogites of the Tauern Window, Austria. *J. Geol.* **87**, 1-27.
- \_\_\_\_\_ (1979b): Experimental determination of the reaction paragonite = jadeite + kyanite + H<sub>2</sub>O, and internally consistent thermodynamic data for part of the system Na<sub>2</sub>O-Al<sub>2</sub>O<sub>3</sub>-SiO<sub>2</sub>-H<sub>2</sub>O, with applications to eclogites and blueschist. *Contrib. Mineral. Petrol.* **68**, 293-301.
- \_\_\_\_\_ & BLUNDY, J. (1994): Non-ideal interactions in calc amphiboles and their bearing on amphibole-plagioclase thermometry. *Contrib. Mineral. Petrol.* **116**, 433-447.
- \_\_\_\_\_ & POWELL, R. (1990): An enlarged and updated internally consistent thermodynamic dataset with uncertainties and correlations: the system K<sub>2</sub>O-Na<sub>2</sub>O-CaO-MgO-MnO-FeO-Fe<sub>2</sub>O<sub>3</sub>-Al<sub>2</sub>O<sub>3</sub>-TiO<sub>2</sub>-SiO<sub>2</sub>-C-H<sub>2</sub>O<sub>2</sub>. *J. Metamorph. Geol.* **8**, 89-124.
- KRETZ, R. (1983): Symbols for rock-forming minerals. *Am. Mineral.* **68**, 277-279.
- LAIRD, J. & ALBEE, A.L. (1981): Pressure, temperature, and time indicators in mafic schists: their application to reconstructing the polymetamorphic history of Vermont. *Am. J. Sci.* **281**, 127-175.
- LEMOINE, M., MARTHALER, M., CARON, M., SARTORI, M., AMAUDRIC DU CHAFFAUT, S., DUMONT, T., ESCHER, A., MASSON, H., POLINO, R. & TRICART, P. (1984): Découverte de foraminifères planctoniques du Crétacé supérieur dans les Schistes Lustrés du Queyras (Alpes occidentales). Conséquences paléogéographiques et tectoniques. *C.R. Acad. Sci. Paris* **299**, 727-732.
- MARUYAMA, S., CHO, MOONSUP & LIOU, J.G. (1986): Experimental investigations of blueschist-greenschist transition equilibria: pressure dependence of Al<sub>2</sub>O<sub>3</sub> contents in sodic amphiboles - a new geobarometer. In *Blueschists and Eclogites* (B.W. Evans & E.H. Brown, eds.). *Geol. Soc. Am., Mem.* **164**, 1-16.
- MASSONE, H.J. & SCHREYER, W. (1987): Phengite geobarometry based on the limiting assemblage with K-feldspar, phlogopite, and quartz. *Contrib. Mineral. Petrol.* **96**, 212-224.
- MONIÉ, P., GALINDO-ZALDÍVAR, J., GONZÁLEZ-LODEIRO, F., GOFFÉ, B. & JABALOY, A. (1991): <sup>40</sup>Ar/<sup>39</sup>Ar geochronology of Alpine tectonism in the Betic Cordilleras (southern Spain). *J. Geol. Soc. London* **148**, 289-297.
- MORIMOTO, N. (1988): Nomenclature of pyroxenes. *Schweiz. Mineral. Petrogr. Mitt.* **68**, 95-111.
- MORTEN, L., BARGOSI, G.M., MARTÍNEZ, J.M.M., PUGA, E. & DÍAZ DE FEDERICO, A. (1987): Meta-gabbro and associated eclogites in the Lubrín area, Nevado-Filábride Complex, Spain. *J. Metamorph. Geol.* **5**, 155-174.
- NIETO, J.M. (1996): *Petrología y geoquímica de los ortogneises del Complejo del Mulhacén, Cordilleras Béticas*. Tesis doctoral, Universidad de Granada, Granada, Spain.
- \_\_\_\_\_, JAGOUTZ, E., PUGA, E. & DÍAZ DE FEDERICO, A. (1997a): Sm-Nd isotopic disequilibrium in eclogites from the Mulhacén Complex (Betic Cordillera, Spain). *Terra Nova, Abstr. Suppl.* **1**, 22.
- \_\_\_\_\_, PUGA, E., MONIE, P., DÍAZ DE FEDERICO, A. & JAGOUTZ, E. (1997b): High-pressure metamorphism in meta-granites and orthogneisses from the Mulhacén Complex (Betic Cordillera, Spain). *Terra Nova, Abstr.* **9**, Suppl. **1**, 22-23.
- PEACOCK, S.M. (1990): Fluid processes in subduction zones. *Science* **248**, 329-337.
- PORTUGAL, M., FERREIRA, J.T., DÍAZ DE FEDERICO, A. & PUGA, E. (1987): Escapolite e biotite hidrotermais e o argon excessivo em rochas básicas das Zonas Internas das Cordilheiras Béticas (Córdoba, Almería) - Origen e papel dos fluidos. *Mem. Not. Univ. Coimbra* **104**, 41-60.
- \_\_\_\_\_, \_\_\_\_\_, PUGA, E. & DÍAZ DE FEDERICO, A. (1988): Geochronological contribution to the petrogenetic picture of the Betic Chain, SE Spain. *II Congreso Geológico de España, Comunicaciones* **2**, 55-58.
- POWELL, R. & HOLLAND, T.J.B. (1988): An internally consistent dataset with uncertainties and correlations. 3. Applications to geothermometry, worked examples and a computer program. *J. Metamorph. Geol.* **6**, 173-204.
- \_\_\_\_\_ & \_\_\_\_\_ (1994): Optimal geothermometry and geobarometry. *Am. Mineral.* **79**, 120-133.

- PUGA, E. (1976): *Investigaciones Petrológicas en Sierra Nevada Occidental*. Tesis doctoral, Universidad de Granada, Granada, Spain.
- \_\_\_\_\_ (1990): The Betic Ophiolitic Association (southeastern Spain). *Ophioliti* **15**, 97-117.
- \_\_\_\_\_ & DÍAZ DE FEDERICO, A. (1978): Metamorfismo polifásico y deformaciones alpinas en el Complejo de Sierra Nevada (Cordillera Bética). Implicaciones geodinámicas. *In Reunión sobre la Geodinámica de las Cordillera Bética y Mar de Alborán*. Universidad de Granada, Granada, Spain (79-111).
- \_\_\_\_\_, \_\_\_\_\_, BARGOSI, G.M. & MORTEN, L. (1989a): The Nevado-Filábride metaophiolitic association in the Cóbdar region (Betic Cordillera, SE Spain): preservation of pillow structures and development of coronitic eclogites. *Geodinamica Acta* **3**, 17-36.
- \_\_\_\_\_, \_\_\_\_\_, BODINIER, J.-L., MONIÉ, P., MORTEN, L. & PORTUGAL, M. (1991): The Betic ophiolitic eclogites (Nevado-Filábride Complex, SE Spain). *In Second Eclogite Field Symp., Abstracts. Terra Nova Abstr.* **3**, Suppl. **6**, 9-10.
- \_\_\_\_\_, \_\_\_\_\_ & DEMANT, A. (1995): The eclogitized pillows of the Betic Ophiolitic Association: relics of the Tethys ocean floor incorporated in the alpine chain after subduction. *Terra Nova* **7**, 31-43.
- \_\_\_\_\_, \_\_\_\_\_, FEDIUKOVA, E., BONDI, M. & MORTEN, L. (1989b): Petrology, geochemistry and metamorphic evolution of the ophiolitic eclogites and related rocks from the Sierra Nevada (Betic Cordilleras, southeastern Spain). *Schweiz. Mineral. Petrogr. Mitt.* **69**, 435-455.
- \_\_\_\_\_, NIETO, J.M., DÍAZ DE FEDERICO, A., BODINIER, J.L. & MORTEN, L. (1999b): Petrology and metamorphic evolution of ultramafic rocks and dolerite dykes of the Betic Ophiolitic Association (Mulhacén Complex, SE Spain): evidence of eo-Alpine subduction following an ocean-floor metasomatic process. *Lithos* **49**, 23-56.
- \_\_\_\_\_, \_\_\_\_\_, \_\_\_\_\_, PORTUGAL, M. & REYES, E. (1996): The intra-orogenic Soportújar Formation of the Mulhacén Complex: evidence for the polycyclic character of the Alpine orogeny in the Betic Cordilleras. *Eclog. Geol. Helv.* **89**, 129-162.
- \_\_\_\_\_, RUIZ CRUZ, M.D. & DÍAZ DE FEDERICO, A. (1999a): Magnetite-silicate inclusions in olivine of ophiolitic metagabbros from the Mulhacén Complex, Betic Cordillera, southeastern Spain. *Can. Mineral.* **37**, 1191-1209.
- ROBINSON, P., SPEAR, F.S., SCHUMACHER, J.C., LAIRD, J., KLEIN, C., EVANS, B.W. & DOOLAN, B.L. (1982): Phase relations of metamorphic amphiboles: natural occurrence and theory. *In Amphibole: Petrology and Experimental Phase Relations* (D.R. Veblen & P.H. Ribbe, eds.). *Rev. Mineral.* **9B**, 1-211.
- SMITH, D.C. (1988): A review of the peculiar mineralogy of the "Norwegian coesite-eclogite Province", with crystal-chemical, petrological, geochemical and geodynamical notes and an extensive bibliography. *In Eclogite and Eclogite-Facies Rocks* (D.C. Smith, ed.). Elsevier, Amsterdam, The Netherlands (1-206).
- SPEAR, F.S. (1993): *Metamorphic Phase Equilibria and Pressure - Temperature - Time Paths*. Mineralogical Society of America, Washington, D.C.
- TENDERO, J.A., MARTÍN-ALGARRA, A., PUGA, E. & DÍAZ DE FEDERICO, A. (1993): Lithostratigraphie des métasédiments de l'association ophiolitique Nevado-Filábride (SE Espagne) et mise en évidence d'objets ankéritiques évoquant des foraminifères planctoniques du Crétacé: conséquences paléogéographiques. *C.R. Acad. Sci. Paris* **316**, Sér. **II**, 1115-1122.
- TORRES ROLDAN, R.L. (1979): The tectonic subdivision of the Betic Zone (Betic Cordilleras, southern Spain): its significance and one possible geotectonic scenario for the westernmost Alpine belt. *Am. J. Sci.* **279**, 19-51.
- TRACY, R.J., ROBINSON, P. & THOMPSON, A.B. (1976): Garnet composition and zoning in the determination of temperature and pressure of metamorphism, central Massachusetts. *Am. Mineral.* **61**, 762-775.
- VISSERS, R.L.M. (1981): *A Structural Study of the Central Sierra de Los Filabres (Betic Zone, SE Spain), with Emphasis on Deformational Processes and their Relation to the Alpine Metamorphism*. Ph.D. thesis, Universiteit Amsterdam, Amsterdam, The Netherlands.
- ZECK, H.P. (1996): Betic-Rif orogeny: subduction of Mesozoic Tethys lithosphere under eastward drifting Iberia, slab detachment shortly before 22 Ma, and subsequent uplift and extensional tectonics. *Tectonophys.* **254**, 1-16.

Received January 20, 2000, revised manuscript accepted September 13, 2000.